Remote Sensing of Environment 233 (2019) 111371

Contents lists available at ScienceDirect

Remote Sensing of Environment

journal homepage: www.elsevier.com/locate/rse

Estimating surface solar irradiance from satellites: Past, present, and future perspectives

Guanghui Huang[a,b,*], Zhanqing Li[c,d], Xin Li[e,f], Shunlin Liang[b], Kun Yang[g], Dongdong Wang[b], Yi Zhang[b]

[a] Key Laboratory of Remote Sensing of Gansu Province and Heihe Remote Sensing Experimental Research Station, Northwest Institute of Eco-Environment and Resources, Chinese Academy of Sciences, Lanzhou 730000, China
[b] Department of Geographical Science, University of Maryland, College Park, MD 20742, USA
[c] Department of Atmospheric and Oceanic Science and ESSIC, University of Maryland, College Park, MD 20740, USA
[d] State Key Laboratory of Remote Sensing Science, College of Global Change and Earth System Science, Beijing Normal University, Beijing, China
[e] Institute of Tibetan Plateau Research, Chinese Academy of Sciences, Beijing 100101, China
[f] CAS Center for Excellence in Tibetan Plateau Earth Sciences, Chinese Academy of Sciences, Beijing 100101, China
[g] Ministry of Education Key Laboratory for Earth System Modeling, Department of Earth System Science, Tsinghua University, Beijing 100084, China

ARTICLE INFO

Keywords:
Surface solar irradiance
Satellites
Radiation budget
Remote sensing
Review

ABSTRACT

Surface Solar Irradiance (SSI) is a key parameter dictating surface-atmosphere interactions, driving radiative, hydrological, and land surface processes, and can thus impinge greatly upon weather and climate. It is thereby a prerequisite of many studies and applications. Estimating SSI from satellites began in the 1960s, and is currently the principal way to map SSI spatiotemporal distributions from regional to global scales. Starting from an overview of historical studies carried out in the past several decades, this paper reviews the progresses made in methodology, validation, and products over these years. First, the requirements of SSI in various studies or applications are presented along with the theoretical background of SSI satellite estimation. Methods to estimate SSI from satellites are then summarized as well as their advantages and limitations. Validations of satellite-based SSI on two typical spatial scales are discussed followed by a brief description of existing products and their accuracies. Finally, the challenges faced by current SSI satellite estimation are analyzed, and possible improvements to implement in the future are suggested. This review not only updates the review paper by Pinker et al. (1995) on satellite methods to derive SSI but also offers a more comprehensive summary of the related studies and applications.

1. Historical background

Surface Solar Irradiance (SSI, ~0.3–4.0 μm), also commonly referred to as surface incident solar radiation, surface downward shortwave radiation, incoming shortwave radiation at the surface, etc., is the primary component of the surface radiation budget (SRB). As a fundamental driving force at the surface, SSI controls water and flux exchanges between the surface and the atmosphere and thus strongly affects other surface processes (e.g., evapotranspiration). On the other hand, negative and positive values of the SRB are compensated by heat fluxes, which in turn cause atmospheric motions at different scales (Mueller et al., 2009). SSI is thus not only of particular importance for modeling land surface processes and assessing Earth's energy disposition (Li et al., 1997a; Stephens et al., 2012), but also necessary for weather and climate predictions and studies of surface-atmosphere interactions. In addition, as clean and renewable energy, it is also indispensable for designing and operating the utilization technologies of solar energy (Zhang et al., 2017).

There are three means of gaining knowledge of SSI: ground observation, numerical modeling and satellite remote sensing (Liang et al., 2019). Each has its merits and deficiencies. Ground observation is the most direct and reliable way to obtain SSI, and measurements those with high-quality instrumentation and maintenance often provide baseline SSI data. For studies and applications that need a stringent data quality, ground observation is still the most indispensable mean. As early as 1964, the World Meteorological Organization (WMO) had set up the World Radiation Data Centre to collect, archive and publish global measurements of SSI and the other SRB components (Kim and Liang, 2010). The well-known Global Energy Balance Archive (GEBA; Wild et al., 2017) currently contains records of ~2500 stations and

* Corresponding author at: 320 Donggang West Road, Lanzhou 730000, China.
E-mail address: luckhgh@lzb.ac.cn (G. Huang).

https://doi.org/10.1016/j.rse.2019.111371
Received 27 September 2018; Received in revised form 12 July 2019; Accepted 13 August 2019

many can extend over several decades. However, point-specific ground measurements are inadequate to characterize the patterns of SSI spatial distributions, especially in remote areas (e.g., sea surface) where observation sites are scarce.

Contrary to ground observation, numerical models (e.g., the general circulation model, GCM) can produce spatiotemporally continuous SSI maps on regional and global scales. Their biggest advantage is their completeness and consistency. This is particularly important for long-term climate monitoring and analysis. Of the various SSI products based on numerical models, reanalysis products are the most common. Typical reanalysis products, such as the Modern Era Retrospective analysis for Research and Applications from the Goddard Space Flight Center (GSFC) and the ERA-Interim reanalysis from the European Centre for Medium-Range Weather Forecasts (Decker et al., 2012), are all widely used. Their major deficiency lies in large errors of models in simulating or predicting cloud quantities. Consequently, the quality of SSI products, especially the high temporal resolution products, is highly questionable (Zhao et al., 2013).

Given its capability of capturing the spatial distribution and dynamic evolution of clouds, satellite remote sensing offers a unique means to monitor and estimate SSI. As such, it has been long recognized that satellite remote sensing is a better way to derive regional and even global SSI than numerical modeling. Many comparative investigations have reinforced the notion that the SSI accuracies in satellite products are higher than those of reanalysis products (Vindel et al., 2016; Zhang et al., 2016; Zhang et al., 2015). The studies in the 1990s have revealed that the estimates of global SSI can be obtained within 28 $W m^{-2}$ (root mean square error, RMSE) or better on a monthly timescale (Li et al., 1995; Pinker et al., 1995). Recent studies have further demonstrated that the uncertainty of satellite-derived monthly SSI may be in the range of the uncertainty of ground observations (Muller et al., 2015; Qin et al., 2011). The majority of discrepancies between satellite-derived and ground-measured SSI are traceable to instrumentation shortcomings (Perez et al., 2017). Therefore, estimating SSI from various satellites is promising to assess regional surface radiation conditions, especially in regions with harsh environments that preclude making routine ground measurements of SSI. Acquiring regional and global SSI data can be divided into two distinct periods: pre-satellite and post-satellite, as pointed out by Li et al. (1997a).

Since the advent of satellite data in the 1960s, numerous efforts have been devoted to developing and improving the satellite-based SSI estimation. This history can be roughly divided into three stages: 1960s to the 1970s, 1980s to the 1990s, and after 2000 (see Fig. 1). In the 1960s and 1970s, pioneering attempts were made to estimate the earth's radiation budget using early weather satellites such as the Television Infrared Observation Satellites (TIROS). TIROS-1 was launched in 1960 and is considered to be the first successful weather satellite. The focus in this stage was mainly on the estimation of the radiation balance of the Earth-atmosphere system (Rasool, 1964). The very first light looming the possibility of estimating the SSI from satellites was shed by Fritz et al. (1964) finding a high correlation (0.9) between satellite observations and ground observation of solar flux. Though Vonderhaar and Suomi (1969) already foresaw the possibility to derive SSI from satellites, the first quantitative estimation of SSI was not made until the late 1970s (Tarpley, 1979). This period is an infancy stage when the concept of SSI remote sensing was proposed, and some experimental/conceptual attempts were made with no practical methods or products generated.

Faster development ensued in the subsequent decades (1980s and 1990s) thanks largely to (1) a new NASA project and a satellite mission, and (2) numerous algorithms proposed during this period. In 1983, the International Satellite Cloud Climatology Project (ISCCP) was established by calibrating and systematically processing data acquired by the narrowband weather satellite sensors onboard U.S. (primary) and international (chiefly Europe) satellites covering the whole globe (Schiffer and Rossow, 1985; Schiffer and Rossow, 1983). Note that these operational sensors operate in narrowband window channels that are least subject to atmospheric absorption so that clouds and surface can be monitored without much interference. However, the solar channels are not calibrated on board. By contrast, broadband calibrated radiative fluxes reflected or emitted by the earth system were measured by the Nimbus-7 and the Earth Radiation Budget Experiment (ERBE). They provided much more accurate measurements of global radiation budget in the entire atmospheric column than any previous missions.

Accompanying these satellite missions was the advent of numerous algorithms to estimate SSI from satellites, as reviewed by Schmetz (1989) and Pinker et al. (1995). Many algorithms were designed for applications with calibrated narrowband data provided by the ISCCP or standalone weather sensors (Gautier et al., 1980; Pinker and Laszlo, 1992; Rossow and Zhang, 1995; Zhang et al., 1995), and some were developed for taking advantage of ERBE broadband measurements (Cess and Vulis, 1989; Chou, 1991; Darnell et al., 1988; Li et al., 1993b). But only a few were used to generate multi-year global SRB products (Li et al., 1993b; Pinker and Laszlo, 1992; Rossow and Zhang, 1995). Two representative examples are the Look-Up Tables (LUTs) based method proposed by Pinker and Laszlo (1992) and the parameterization method developed by Li et al. (1993b) (see Section 3 for details).

It was not until the satellite-estimation made in the 1990s that drastically altered our conventional knowledge of the global mean Solar Surface Radiation Budget (SSRB) from > 180 $W m^{-2}$ to ~160 $W m^{-2}$. Li et al. (1997a) compared three SSRB products together with model values from four GCMs, and found that the models produced systematically higher mean SSRBs than the satellite estimates. The model results agreed more or less with the conventional wisdom, namely, that the global earth surface absorbs ~180–190 $W m^{-2}$, whereas the satellite estimates ranged from 157 $W m^{-2}$ (Li et al., 1993a) to 171 $W m^{-2}$ (Pinker and Laszlo, 1992). The value obtained by Li et al. (1993a) grossly agreed with later estimates of 160–165 $W m^{-2}$ (Loeb and Wielicki, 2016; Stephens et al., 2012; Wild et al., 2013).

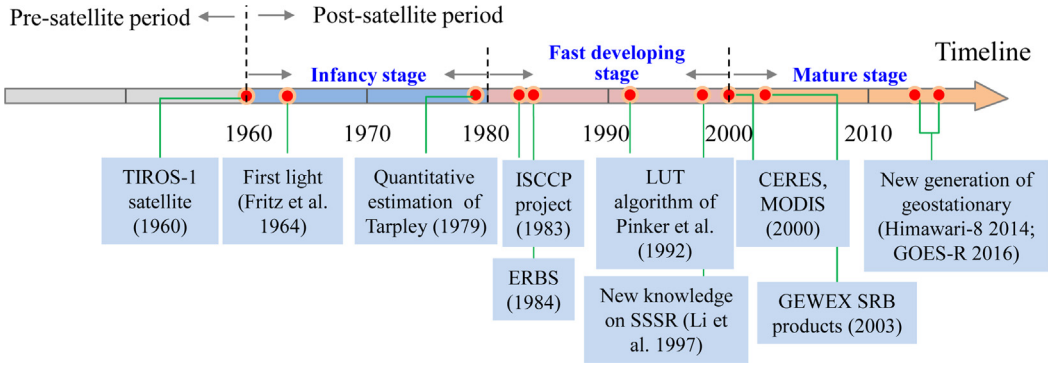

Fig. 1. Schematic showing the history of SSI satellite estimation.

After 2000, satellite-based estimation of SSI and other SRB components had become increasingly mature thanks partially to the modern satellite sensors that have onboard calibration for both narrow and broadband channels, as well as further development of remote sensing methods (e.g. Huang et al., 2016b; Kim and Liang, 2010; Ma and Pinker, 2012; Tang et al., 2016; Zhang et al., 2018). Many sensors of the new century, such as the Moderate Resolution Imaging Spectroradiometer (MODIS) and Clouds and the Earth's Radiant Energy System (CERES) of NASA's Earth Observation System, employed an onboard radiometric calibration system to quantify observations, which is thought to be a more effective and accurate way for calibration.

Besides the advances in sensors, many more sophisticated algorithms have been developed in which detailed radiative transfer processes are considered (Huang et al., 2016b; Huang et al., 2011; Kim and Liang, 2010; Tang et al., 2016; Zhang et al., 2018). In these algorithms, multi-channel satellite observations are frequently combined to more quantitatively determine the states of the atmosphere and surface (Huang et al., 2016b; Kim and Liang, 2010; Zhang et al., 2018). Multi-source satellite data are also combined to compensate for each other's shortcomings (Huang et al., 2011; Tang et al., 2016).

With the development of quantitative remote sensing technology, more satellite-based products regarding aerosols, water vapor, ozone etc. have become or are becoming available (e.g., various MODIS products), which may provide better inputting choices for the generation of regional or even global SSI products than traditional climatological data (Bisht and Bras, 2010; Bisht et al., 2005; Huang et al., 2012; Van Laake and Sanchez-Azofeifa, 2004). Also during this period, answers to some scientific questions in history are becoming increasingly clear. For example, the historical debate (once fervent in the 1990s) on the attribution of large reduction in SSRB or big increase in atmospheric absorption, eventually ended up with a consensus that the reduction was caused chiefly by underestimation of absorption by water vapor and aerosols (Li et al., 2003; Li et al., 2004), not the so-called cloud absorption anomaly as was once claimed (Cess et al., 1995; Ramanathan et al., 1995).

It has been 25 years since the last comprehensive review on SSI was published (Pinker et al., 1995). An update on later progress is long overdue given the recent fast and extensive development in the remote sensing of SSI. The main objective of the review provided here is to summary SSI studies with a focus on methods, validations, and data products, and gain insight on the current status of the remote sensing of SSI. Also discussed are the outlooks of future developments and improvements.

2. Requirements for SSI and the theoretical background of SSI satellite estimation

2.1. Requirements for SSI in various applications or study areas

Different applications and studies have diverse requirements for SSI with respect to its spatial resolution, timescale, coverage, and quality levels. In climate-monitoring-related areas, long-term, consistent, and calibrated SSI data are always needed (Ma and Pinker, 2012). In global change research areas, features like global coverage (especially including the Arctic, the Antarctic, the Tibet Plateau and other hotspots) and data homogeneity are more emphasized (Hollmann et al., 2006). For energy balance and water cycle studies at catchment scales, SSI is expected to obtain at an hourly timescale and at a resolution of several kilometers (Li et al., 2016; Margulis et al., 2006). For solar energy applications, SSI is needed at finer spatial resolutions (e.g., satellite pixel) and at a range of temporal resolutions (Perez et al., 2013; Zhang et al., 2017), and so is for evapotranspiration modeling based on remote sensing data (Liu et al., 2016; Xu et al., 2015).

Table 1 lists the quantitative user-defined requirements for SSI in the application areas of the WMO, i.e., areas related to weather, water and climate, which are collected by the WMO Observing System Capability Analysis and Review Tool (OSCAR, a resource developed by the WMO in support of Earth Observation applications, studies and global coordination: https://www.wmo-sat.info/oscar/variables/view/50). The requirements are divided into three grades: “goal”, “breakthrough”, and “threshold”. The “threshold” grade is the lowest quality level that one application can accept. The table shows that the spatio-temporal features of the needed SSI vary greatly not only from one application to another but also between the different grades.

Diverse SSI products with different features (spatial resolutions, temporal cycles, accuracy criteria, etc.) are thus required to meet various application needs. Accordingly, a large number of studies have been published over the past several decades on this topic. These studies were motivated differently and span a wide range of complexity. It is impossible and unnecessary to review all of them, but a few are selected for illustration purposes.

2.2. The theoretical background of SSI satellite estimation

Fig. 2 outlines the relations between satellite observations and SSI under the approximation of a plane-parallel atmosphere for clear and cloudy skies. Satellites observe the top-of-atmosphere (TOA) two-way reflectance (or radiance) of the Earth-atmosphere system, whereas SSI is mainly determined by the radiative attenuations caused by different atmospheric constituents, and to a lesser degree, by the surface albedo. So in principle, the atmospheric constituents' loadings should first be retrieved directly or indirectly from satellite TOA observations then subsequently used to infer the solar irradiance that finally arrives at the surface. However, as shown by Fig. 2, satellite TOA observations usually contain integrated information from both the atmosphere and the surface. Retrievals always face the challenge of how to decouple them.

Of the various atmospheric constituents under clear-sky conditions, ozone, water vapor, and aerosols are three critical components because of their influences on SSI and their variability in the atmosphere. Ozone and water vapor absorb solar radiation at certain wavelengths, which means that their loadings can be effectively retrieved by the sharp contrasts between the absorption windows and the nearby non-absorption windows (Bhartia et al., 1996; Gao and Kaufman, 2003; Liu et al., 2017). Consequently, various ozone and water vapor satellite products, e.g., Total Ozone Mapping Spectrometer (TOMS) ozone products and MODIS water vapor products, are generally reliable for estimating SSI.

Compared to ozone and water vapor, aerosols are more challenging to retrieve. Particularly over land, the quantitative retrieval of aerosols is still fraught with difficulties due to various factors such as cloud contamination, differentiation of reflection by aerosols and surface, and aerosol properties, as reviewed by Li et al. (2009). For example, the conventional and operational “dark target” strategy can only be successfully implemented over dark land surfaces (Kaufman et al., 1997; Levy et al., 2007). As the surface brightens, decoupling aerosol optical depth (AOD) and surface reflectance from TOA reflectance becomes increasingly difficult because of the worsening stability of the solution space (Huang et al., 2015). Therefore, though there are some specialized algorithms for bright surfaces (e.g., Hsu et al., 2013), AOD retrievals over bright surfaces are still questionable and inferior to those over dark surfaces (Lyapustin et al., 2011).

As the strongest modulator of SSI (far stronger than other atmospheric constituents), clouds play a pivotal role in estimations of SSI. In view of the decisive influence of clouds on SSI, to some extent, SSI satellite estimation is conducted around how to accurately account for radiative attenuation by clouds (cloud scattering and absorption) in the atmosphere. Towards this end, there are two different strategies: 1) directly inferring the attenuation of clouds and subsequently SSI from TOA satellite observations, or 2) estimating the attenuation of clouds and SSI based on satellite cloud products that are already derived from raw satellite data. Unlike Rayleigh scattering and scattering by aerosols,

Table 1
Quantitative requirements for SSI collected by WMO OSCAR in weather, water, and climate related areas (*Goal*: an ideal requirement above which further improvements are not necessary; *Break.*: an intermediate level which, if achieved, would result in a significant improvement for the targeted application; *Thres.*: the minimum requirement to be met to ensure that the SSI data are useful).

Application areas	Spatial resolution			Temporal scale			Uncertainty (RMSE)		
	Goal	*Break.*	*Thres.*	*Goal*	*Break.*	*Thres.*	*Goal*	*Break.*	*Thres.*
Global NWP[a]	10 km	30 km	100 km	60 m	3 h	12 h	1 W m^{-2}	10 W m^{-2}	20 W m^{-2}
Agricultural meteorology	1 km	5 km	20 km	24 h	2 d	7 d	–	–	–
Nowcasting and VSRF[b]	5 km	15 km	50 km	60 s	10 m	60 m	1 W m^{-2}	10 W m^{-2}	20 W m^{-2}
Climate monitoring	25 km	50 km	100 km	24 h	2 d	5 d	5 W m^{-2}	6.5 W m^{-2}	10 W m^{-2}

[a] NWP: Numerical Weather Prediction.
[b] VSRF: Very Short Range Forecasting.

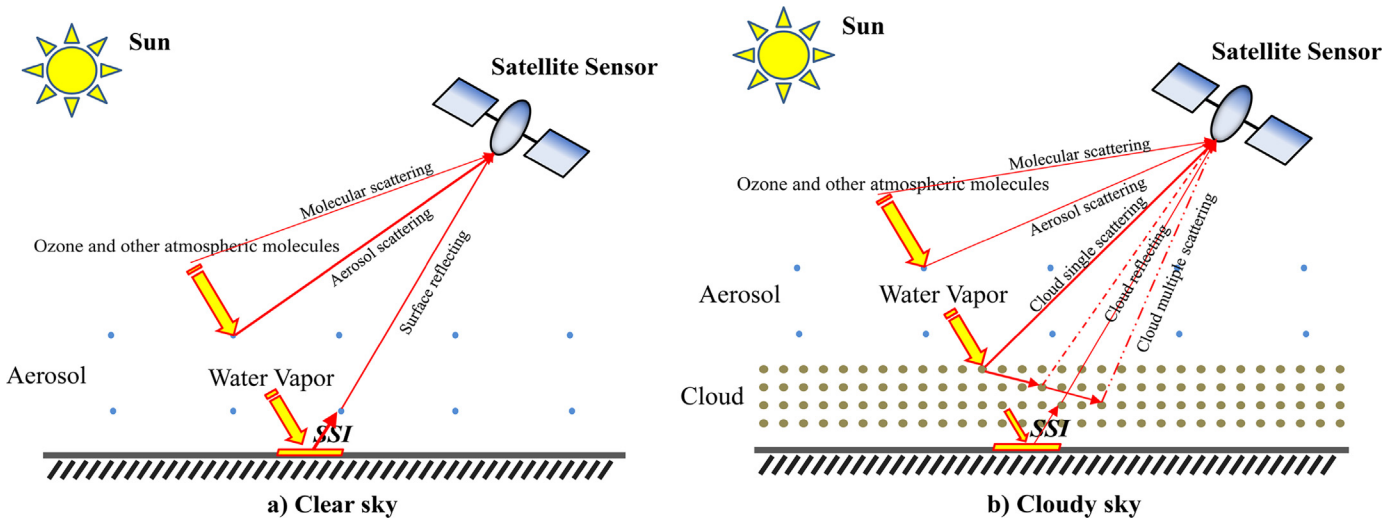

Fig. 2. Simplified relations between satellite observations and SSI according to one-dimensional radiative transfer theory for a) clear sky and b) cloudy sky.

multiple scattering dominates in clouds (see Fig. 2). This is an intractable issue and in radiative transfer theory, usually involves complex numerical procedures that are difficult to understand and implement (Mayer et al., 2016). Therefore, both strategies face the difficulty of how to develop a more operational and convenient approach to circumvent these numerical procedures, but with little degradation in accuracy.

In addition, clouds change dramatically in space and time. To effectively capture their spatial patterns and dynamic evolution, high temporal resolution geostationary data are of particular importance in satellite-based SSI estimations.

3. Estimation of SSI from satellites

As mentioned in Section 2.1, many algorithms to estimate SSI from satellite data have been developed over the past several decades. From the methodology point of view, they can be roughly grouped into two categories: methods based on radiative transfer processes and statistical methods.

3.1. Methods based on radiative transfer processes

Detailed radiative transfer in the atmosphere is a complex problem (Liou, 2002). It involves the acquisition of atmospheric spectral properties and the development of radiative transfer equation solvers. Therefore, it is costly and even unrealistic to run complicated radiative transfer models (RTMs) like the MODerate resolution atmospheric TRANsmission (MODTRAN) or LibRadtran (Emde et al., 2016; Mayer and Kylling, 2005) to compute the SSI. Conversely, the core idea of methods based on radiative transfer processes is how to reduce the spectral dependence (using proper broadband modes) and simplify the radiative transfer solution while retaining the accuracy as much as possible.

3.1.1. LUT-based methods

LUT-based methods use offline two-way LUTs to simplify radiative transfer processes and subsequently retrieve SSI. The so-called "two-way LUT" emphasizes that the information along the solar-to-surface path and the information along the surface-to-TOA path are both stored in LUTs. Such methods usually contain the following two steps: 1) the relationships between TOA albedos or reflectance and atmospheric transmittances are established in the form of LUTs through extensive radiative transfer simulations for different atmospheric conditions, and 2) SSI is then estimated by matching one given satellite TOA observation and the predefined LUT values.

Fig. 3 presents the flowchart of the broadband LUT algorithm proposed by Pinker and Laszlo (1992). Narrowband bidirectional reflectance observed by geostationary satellites is first transformed into broadband bidirectional reflectance; and the broadband bidirectional reflectance is then converted into TOA broadband planetary albedo using the angular distribution model based on the ERBE satellite. The resulting TOA broadband planetary albedo serves as the starting point of the algorithm to infer the transmission-reflection function by matching it with the values stored in the LUTs for different atmospheric and surface states. The broadband LUT algorithm of Pinker and Laszlo (1992) has been widely used to generate global gridded SSI products. For example, the Global Energy and Water cycle Exchanges (GEWEX) project uses its modified version as the primary algorithm for producing the GEWEX SRB global product. Ma and Pinker (2012) used an updated version of the algorithm to produce the new University of Maryland

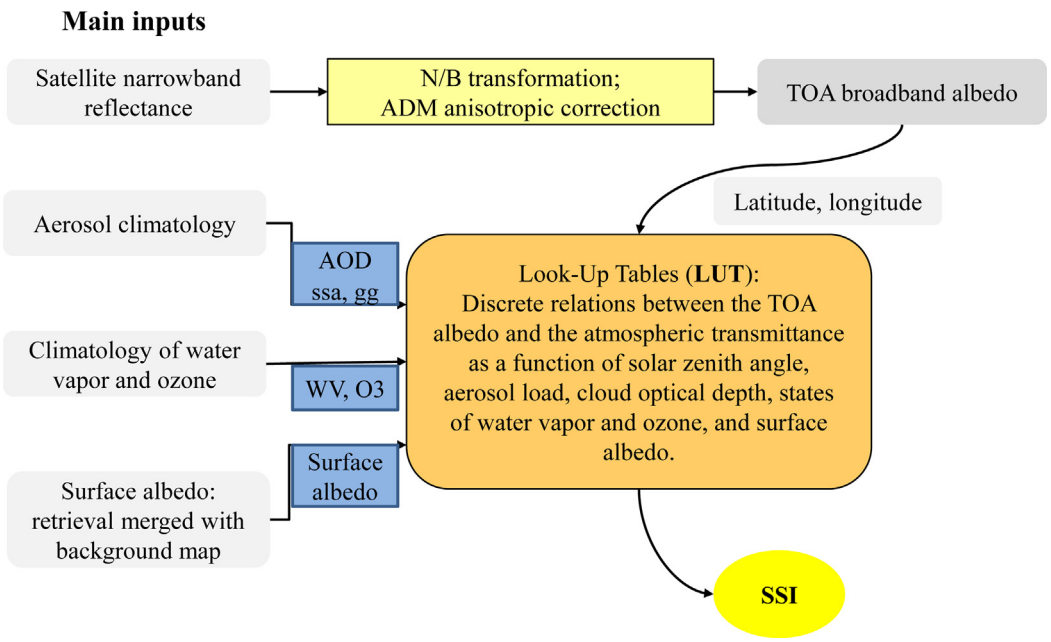

Fig. 3. Diagram of the broadband LUT algorithm proposed by Pinker and Laszlo (1992) (*ssa*: single scattering albedo; *gg*: asymmetric factor; N/B: narrowband to broadband; ADM: angular distribution model).

(UMD) SRB global dataset (see Table 3 in Section 5.2 for details). Based on this algorithm, the EUMETSAT Satellite Application Facility on Climate Monitoring (CM SAF) generated global long-term SSI maps from the Advanced Very High Resolution Radiometer (AVHRR) data (Mueller et al., 2009; Trentmann and Kothe, 2016).

On the other hand, SSI can also be directly retrieved from a narrowband satellite channel using a similar retrieval scheme, namely, narrowband LUT algorithms. Here, the TOA narrowband bidirectional reflectance observed by satellites is directly linked with SSI using a set of more detailed LUTs that are created by radiative transfer modeling (Huang et al., 2016b; Huang et al., 2011; Liang et al., 2006; Lu et al., 2010). One of the earliest narrowband LUT algorithms was developed by Liang et al. (2006), who retrieved surface photosynthetically active radiation (PAR, ~0.4–0.7 μm) by establishing LUTs between the MODIS blue channel and PAR at the surface. The MODIS blue channel is generally considered sensitive to aerosols, so their LUTs implicitly include the explanations for aerosols and clouds. Following Liang et al. (2006), Lu et al. (2010) and Huang et al. (2011) developed their narrowband SSI retrieval algorithms, which are based on the Geostationary Meteorological Satellite 5 (GMS-5) visible channel and the Multifunctional Transport Satellites (MTSAT) visible channel, respectively. But because the GMS-5 and MTSAT visible channels are both insensitive to aerosol loading over land surfaces, only the influences of clouds were considered in these LUTs. Using a similar algorithm, Zhang et al. (2014) produced a set of experimental global high-resolution (~5 km) SSI and PAR datasets covering 2008 to 2010.

In addition to single-channel algorithms, there are a few multi-channel-based algorithms that use information from two or more satellite-observing channels. For instance, Huang et al. (2016b) improved their LUT algorithm based on a geostationary satellite visible channel by importing the thermal infrared channel to distinguish between ice clouds and water clouds. Zhang et al. (2018) proposed an optimized LUT algorithm to retrieve SSI from the first seven MODIS channels by defining a cost function.

In the LUT-based methods, determining the surface states (surface albedo or reflectance) is a critical prerequisite. In general, for broadband LUT algorithms, the surface albedo is determined according to the collective information of the background surface types and the narrowband surface reflectance estimated from clear-sky satellite observations. For narrowband LUT algorithms, the narrowband surface reflectance is calculated using clear-sky satellite observations or the minimum reflectance technique. The so-called minimum reflectance technique utilizes the fact that the minimum TOA reflectance during a certain time window always represents a clear case and even the clearest case (the lowest aerosol load).

LUT-based methods provide a direct SSI retrieval strategy from raw satellite data and avoid the need for atmospheric state parameters (e.g., cloud property parameters). They are thus suitable for SSI retrievals when satellite-based atmospheric products are unavailable. Of course, if these parameters, as well as the surface albedo, are already known, two-way LUTs can also reduce into the simpler one-way mode, that is, only information about the solar-to-surface path is used to estimate SSI (Deneke et al., 2008). However, such LUT-based algorithms are uncommon. Since the LUT is a close approximation to a complicated RTM, in theory, LUT-based algorithms should be accurate. Their weakness is that this kind of algorithm is usually computationally inefficient and strongly sensor-specific. Also, not all radiative extinction processes are accounted for in LUTs for the sake of efficiency.

3.1.2. *Simplified RTM-based methods*

If the needed atmospheric parameters as well as the surface albedo have been derived from raw satellite data, they can be straightforwardly fed into a simplified RTM to estimate SSI. Here, the simplified RTM (suitable for irradiance or flux calculations) serves as a forward SSI inference scheme, driven by satellite-based atmospheric and surface state information. For example, ISCCP gridded cloud datasets as well as other ancillary data are input into the NASA Goddard Institute for Space Sciences (GISS) RTM to produce the global ISCCP flux dataset (Zhang et al., 2004).

Compared with complicated spectral RTMs, the simplified RTMs involve the simplification of spectral modes and the choice of a simpler radiative transfer solution. A simplified RTM is thus usually assembled with a broadband spectral parameterization and a fast RTM solver for irradiance calculations. The simplified RTM-based methods generally contain three processes. Different atmospheric state parameters like the ozone profile, surface pressure, and cloud microphysical parameters are first converted into their individual optical properties. These optical properties are then integrated and the integrated atmospheric optical

property is input into a fast RTM solver to obtain SSI. Of the various RTM solvers, the two-stream approximation and its derivatives are preferred because they have definite analytical solutions. In particular, tuned two-stream approximations like the δ-two-stream approximation or its variants like the δ-Eddington approximation are generally thought of as suitable solvers to approximate irradiance (Briegleb, 1992; Raisanen, 2002), and are thus frequently used to estimate the surface irradiance or flux. For instance, based on the δ-Eddington approximation, Wang and Pinker (2009) developed a new algorithm to infer fluxes in seven spectral intervals at the surface as well as the given atmospheric layers. CERES Level 3 SYN1deg products utilize a classic δ-two-stream algorithm to estimate SSI in 15 shortwave spectral bands from 0.2 to 4.0 μm (https://ceres.larc.nasa.gov/science_information.php?page=CeresComputeFlux).

The simplified RTM-based methods have very solid physical basis, and their accuracies are contingent on the quality of the input parameters to some extent. The availability of reliable atmospheric products (retrieved from satellite observations or provided by various auxiliary data, or both) thus appears more important in such methods. One of their disadvantages is that simplified RTMs are more complicated than other methods.

3.1.3. Parameterization methods

Following the same philosophy, SSI can also be estimated using various parameterization schemes provided that satellite-based atmosphere as well as surface state information is known. These parameterization schemes generally consist of schemes for clear skies and parameterizations of clouds. In clear-sky parameterization schemes, the absorption of permanent gases, ozone absorption, water vapor absorption, Rayleigh scattering, and aerosol scattering are often parameterized separately. This means that the radiative extinctions caused by various atmospheric constituents are treated independently. Such a strategy is different from that of simplified RTM-based methods, where the integrated optical property of all atmospheric constituents is first obtained then fed into the simplified RTMs.

Since there have already been many parameterizations of the radiative extinctions due to different atmospheric constituents (Gueymard, 2003a, 2003b; Slingo, 1989; Stephens et al., 1984; Yang et al., 2001; Yang et al., 2006b), recent studies have mainly focused on how to combine them with various atmospheric products and surface products that are derived from new satellites to obtain new SSI (Bisht and Bras, 2010; Bisht et al., 2005; Huang et al., 2012; Qin et al., 2015; Van Laake and Sanchez-Azofeifa, 2004). For instance, Van Laake and Sanchez-Azofeifa (2004) used the clear-sky parameterization scheme of Iqbal (1983) and the cloud parameterization of Stephens et al. (1984) to calculate surface incident PAR from MODIS atmospheric products. Bisht et al. (2005) developed a more empirical parameterization algorithm for estimating SSI under clear-sky conditions using the MODIS atmospheric profile product, and then further extended it to all-sky conditions by importing the cloud parameterization of Slingo (1989) and more MODIS products (Bisht and Bras, 2010). Also based on MODIS products, Huang et al. (2018) developed a new broadband parameterization to estimate all-sky SSI.

We regard the above methods as general parameterization methods. General parameterization methods are a simple and efficient way to estimate SSI. The feature that various radiative extinctions caused by different atmospheric constituents are accounted for separately has at least two advantages: 1) a certain physical basis and 2) the ability to quickly identify problems when poor estimates of SSI occur. The challenge of such methods lies in their explicit requirements for atmosphere and surface parameters. As mentioned in Section 2.2, some needed parameters are so difficult to retrieve because of inherently ill-posed retrieval problems (Holz et al., 2016; Levy et al., 2010) that their retrieval uncertainties generally are much larger than that of SSI itself.

However, there is another school of parameterization methods that can implicitly infer SSI from TOA satellite observations (Ciren and Li, 2003; Li et al., 1993a; Li et al., 1993b; Li and Moreau, 1996; Li et al., 2000; Moreau and Li, 1996). Li et al. (1993b) found there is a simple relation between net surface solar irradiance (can be abbreviated as NSSI) and TOA albedo, which is only significantly affected by water vapor in the atmosphere. NSSI (a simple function of SSI and surface albedo) can, therefore, be inferred by a parameterization in which only water vapor is explicitly imported. The foundation of the parameterization lies in the fact that the most influential variables driving TOA irradiance also dictates surface irradiance, especially scattering by clouds which reduce NSSI at the expense of increase in reflection at TOA as measured by satellite. The challenging task of inferring cloud variables is thus circumvented. The same principle has been applied to the retrievals of PAR (Li et al., 1993a; Li and Moreau, 1996; Li et al., 1997b) and ultraviolet radiation (Ciren and Li, 2003; Li et al., 2000; Wang et al., 2000) having an even higher accuracy, thanks to the fact that clouds and water vapor have no absorption in these bands.

The parameterizations developed by Li and colleagues avoid the ill-posed retrieval problem for they have fewer input parameters than the full-fledged radiative transfer models have. They are more convenient due to the minimum demands for information about the atmosphere, cloud and the surface. The limitation is that only NSSI can be directly retrieved. One can, however, easily derive SSI by knowing surface albedo. The parameterization scheme of Li et al. (1993a) has been employed by the CERES to generate the instantaneous global SRB products.

3.2. Statistical methods

Besides physical methods and physics-based parameterization methods, there are many statistical methods used to estimate SSI. According to the specific statistical relationships used in these methods, statistical methods can be divided into conventional statistical methods and statistical optimization methods. A variety of machine-learning methods are most representative of the latter.

3.2.1. Conventional statistical methods

Conventional statistical methods adopt experience-based statistics functions to connect satellite observations and SSI. These methods usually use the fact that the TOA reflectance measured by satellites is approximately proportional to the cloud transmission. Among these methods, the most famous is perhaps the Heliosat method (Cano et al., 1986; Qu et al., 2012; Rigollier et al., 2004).

In the early Heliosat method, the clear-sky SSI was first calculated via an empirical model where the atmospheric transmittance was deemed to be a function of the Linke turbidity factor. Then a cloud index (n) and a clear-sky index (k_T^*) was introduced to characterize the amount of cloudiness and the cloud radiative extinction, respectively. They are defined as (Rigollier et al., 2004)

$$n = \frac{\rho - \rho_{clr}}{\rho_{\max} - \rho_{clr}} \tag{1}$$

and

$$k_T^* = \frac{G}{G_{clr}}, \tag{2}$$

where ρ is the apparent reflectance observed by satellites (note that the term “reflectance” is often misused as “albedo” in many Heliosat-related articles). $\rho_{\max}$ is the apparent reflectance of the brightest clouds and ρ_{clr} is the apparent reflectance under clear skies. G and G_{clr} are the actual surface irradiance and the clear-sky irradiance, respectively. Finally, the two variables are correlated to each other in a statistical relationship (shown in Fig. 4) and the SSI under all-sky conditions can be derived. The Heliosat method was originally proposed by Cano et al. (1986) and later modified by many others (e.g., Beyer et al., 1996; Qu et al., 2012; Rigollier et al., 2004). Currently, it has been updated to the forth version (Heliosat-4), and among different versions there are slight

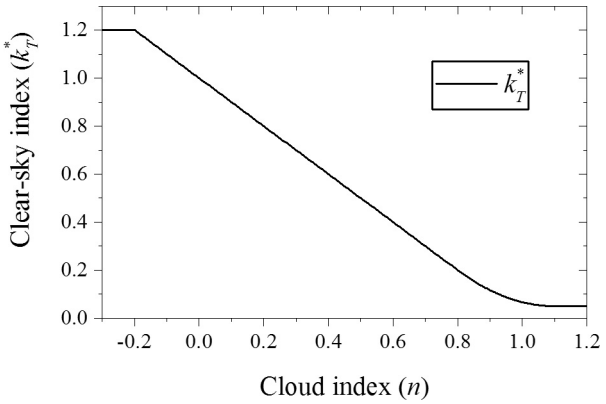

Fig. 4. The clear-sky index k_{T^*} (cloud transmission) is treated as a segmentation function of cloud index (n) in the Heliosat method (Hammer et al., 2003).

difference.

Similar methods are frequently applied for solar energy applications. For example, Perez et al. (2002) developed an operational satellite model (with basically the same steps as Heliosat), which evolved over years into the SUNY model and the SolarGIS model. They are the engines of commercial SSI products of SolarAnyWhere and SolarGIS (Perez et al., 2015).

In spite of their experiential nature, statistical methods generally have a good accuracy for their fundamental nature of "tuning" against surface measurements. As pointed out by Perez et al. (2013), even using short-term surface data to calibrate the methods, their long-term accuracies are substantially improved. This kind of methods is often used to produce industry SSI products for solar energy applications.

3.2.2. Machine Learning (ML) based methods

ML-based methods are similar to conventional statistical methods, but here, various machine-learning techniques act as bridges between satellite observations and SSI. Machine-learning techniques that are often used for SSI estimation include artificial neural networks (ANN), support vector machine/support vector regression (SVM/SVR), Bayesian networks (BN), decision tree learning (DTL) etc. (Aguiar et al., 2015; Akarslan and Hocaoglu, 2016; Voyant et al., 2017). Of these machine-learning techniques, ANN is most common in the literature. As an example, next the model of Linares-Rodriguez et al. (2013) is introduced.

An ANN-based model is generally comprised of three layers, i.e., input layer, hidden layer, and output layer. The input layer (independent vector) of the model of Linares-Rodriguez et al. (2013) includes 11 channels of the Spinning Enhanced Visible and Infrared Imager (SEVIRI) instrument plus a clear-sky term G_{cs} that represents SSI under clear skies. The hidden layer consists of 25 neurons and an activation function to standardize the inputs to the range of $[-1, 1]$. In the output layer (dependent vector), a linear activation function is adopted to implement the prediction of all-sky SSI. In their paper, measurements from 65 out of 83 stations across the Andalusian region in Spain were used for training the model (the remaining 18 were for testing) and daily SSI with a relative RMSE of 6.8% were finally produced.

There are a huge number of similar papers published in the five main journal for solar energy application studies (*Applied Energy, Energy, Energy Conversion and Management, Renewable Energy, and Solar Energy*) (Aguiar et al., 2015; Akarslan and Hocaoglu, 2016; Akarslan et al., 2014; Janjai et al., 2009; Mefti et al., 2008) that have recently been reviewed (Voyant et al., 2017; Zhang et al., 2017). Machine-learning is a subfield of computer science and is classified as an artificial intelligence method (Voyant et al., 2017). The advantage of this kind of method is that it can solve some obscure problems in which the mapping from the independent vector to the dependent vector cannot be represented by explicit functions. But owing to the lack of a physical basis, the representativeness of such methods highly depends on the

Table 2
Summary of methods for estimating SSI from satellites.

Usual algorithms	Main inputs	Advantages	Limitations	References
LUT-based methods				
Broadband algorithms; narrowband algorithms; multichannel algorithms	1) TOA reflectance or radiance; 2) Auxiliary atmospheric data	1) A direct SSI retrieval strategy; 2) Accurate in theory	1) Computationally inefficient; 2) Sensor-specific 3) Linear interpolation	Pinker and Laszlo (1992); Huang et al. (2011)
Simplified RTM methods				
δ-2-stream approximation; δ-Eddington approximation	Integrated atmospheric optical properties and surface optical properties (albedo or reflectance)	1) Solid physical basis; 2) Accurate in theory; 3) Independent of specific sensors	1) Requires reliable optical input parameters on atmosphere and surface 2) Higher complexity	Zhang et al. (2004); Wang and Pinker (2009)
Parameterization methods				
General parameterization	1) Satellite-based atmospheric and surface products; 2) Auxiliary data	1) Simple; 2) Certain physical basis; 3) Easy to determine the reasons for poor estimates	1) Explicit requirements for various atmosphere and surface state parameters 2) Quality products of some parameters are unavailable	Bisht and Bras (2010); Huang et al. (2018)
Parameterization of Li and colleagues	1) TOA planetary albedo; 2) Water vapor	1) A direct strategy 2) Convenient; 3) Minimum demand for information	NSSI not SSI is directly retrieved	Li et al. (1993a, 1993b); Li et al. (2000); Wang et al. (2000)
Conventional statistical methods				
Heliosat algorithm; SUNY algorithm	1) TOA reflectance or radiance; 2) Other auxiliary data	1) Simple; 2) Efficient	1) Lack of physical basis; 2) Sensor-specific; 3) Possibly needs calibrations over different regions	Rigollier et al. (2004); Perez et al. (2013)
Machine Learning based methods				
SVM/SVR algorithms; BN algorithms; DTL algorithms	1) TOA reflectance or radiance; 2) Various other information dependent on specific algorithms	1) Efficient; 2) Non-linear relationship	1) Lack of physical basis; 2) Sensor-specific; 3) Dependent on training data and representativeness problem	Linares-Rodriguez et al. (2013); Voyant et al. (2017)

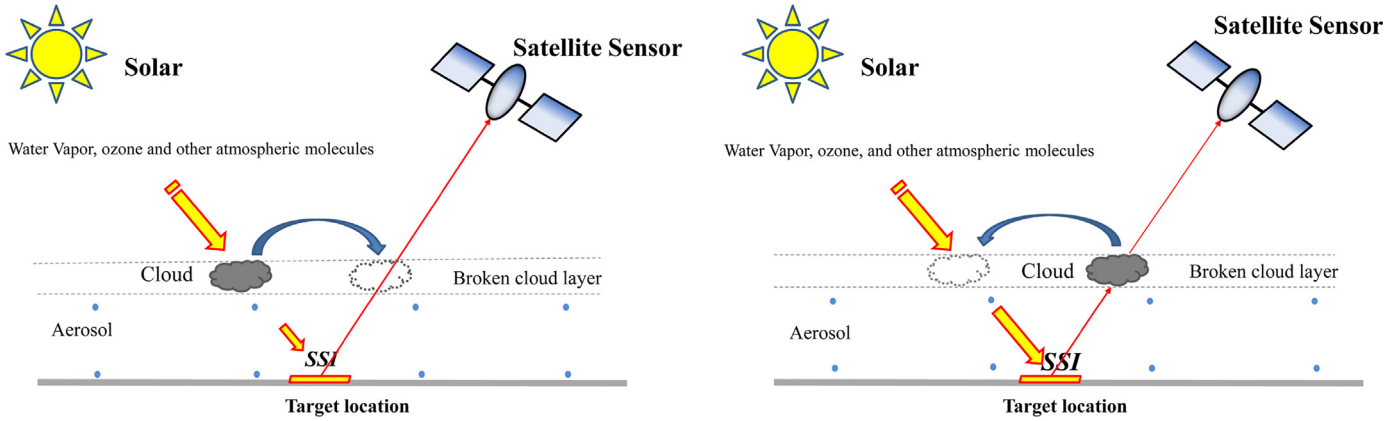

Fig. 5. Illustration of misleading atmospheric condition (clear or cloudy) observed by the satellite sensor: a) when a cloud only exists in the sun-to-surface path and b) when a cloud only exists in the surface-to-satellite path.

training data and consequently, their generalizability is limited. Though occasionally adopted to estimate instantaneous SSI (Kim and Liang, 2010), statistical methods are more frequently used to estimate SSI on longer timescales such as daily, monthly, or yearly.

3.3. Comparison of different methods

For a concise overview, Table 2 summarizes the needed input data, advantages, limitations, and representative literature for each method previously discussed. Because of their different nature, input requirements, and operability, there is no general conclusion on which method is superior to others. Likewise, a quantitative summary of the accuracies of different methods is difficult to conclude. As for the choice of an optimal method, one must comprehensively consider the sensor characteristics, the availability of reliable atmospheric products and surface observation, and the expected timescale of SSI. For scientific research and application, physical methods are in favor, and vice versa for solar energy application. Of course, this is not an either-or choice. Actually in many operational algorithms two or more kinds of methods are often combined. For example, in Heliosat-4 (Muller et al., 2015) the physical LUT method for clear skies and Heliosat empirical relationships for cloudy skies are combined to calculate the all-sky SSI. The operational algorithms developed by Mueller et al. (2009) imported various parameterizations to reduce the computational burden under the framework of the broadband LUT method of Pinker and Laszlo (1992). The international energy agency Solar Heating and Cooling Project Task 4 "Solar Resource Assessment and Forecasting" is also addressing the objective of advancing solar SSI modeling based on physical principles (http://task46.iea-shc.org/).

4. Validations of satellite-based SSI

We usually use in-situ measurements to validate satellite-based SSI products including high-resolution kilometer-scale products and coarse-resolution gridded products. However, the discrepancy between in-situ measurements and collocated estimates of satellite-based SSI may not denote the true error of satellite products (Li et al., 1995), because many factors may contribute to it (Wang et al., 2016). These factors not only may result in considerable validation uncertainties, but in turn affect our validation strategies to some extent, as elaborated in more details next.

4.1. Validations of the high-resolution SSI

For the validation of high-resolution SSI (generally consistent with the native resolution of satellite observations, i.e., about several kilometers), many studies (Deneke et al., 2009; Huang et al., 2016a) have shown that the 3D effect of clouds may affect validation results significantly with increasing temporal resolutions. Especially for the instantaneous products, the uncertainty originating from the 3D effect of clouds is very large.

First, the 3D effect of clouds makes instantaneous surface measurements more unstable and thus lowers their representativeness (Huang et al., 2016a). Second, inhomogeneous cloud fields lead to a smoother SSI beneath clouds compared with that retrieved by conventional algorithms (based on the 1D radiative transfer theory for a plane parallel atmosphere) due to the strong adjacent effect of pixels (Wyser et al., 2005; Wyser et al., 2002). A simple way to mitigate the impact of the 3D effect of clouds on the validation of instantaneous SSI, is through temporal averaging of surface measurements and spatial averaging of satellite-based SSI estimates (Wyser et al., 2002).

Based on a multi-resolution analysis of 5-min resolution atmospheric transmittance and geostationary TOA reflectance, Deneke et al. (2009) recommended a 40–60 min averaging interval for surface measurements to validate the instantaneous SEVIRI pixel-level (6 km × 3 km) SSI products. In an investigation into validation uncertainty using a dense matrix of surface observations, Huang et al. (2016a) suggested that a 30-min averaging interval instead of smaller time intervals is the most optimal timescale for the validation of instantaneous 5-km resolution satellite retrievals. This is because the higher frequency surface measurements likely contain more detailed cloud information on a sub-pixel scale not captured by satellite observations. After comparing the SSI output from a 3D Monte Carlo RTM and that from a conventional 1D RTM for the same simulated cloud fields, Wyser et al. (2005) showed that a spatial averaging of $\geq$5 km can dramatically reduce the impact of the 3D effect of clouds and that the optimal spatial size is ~25 km. So, in the validation of instantaneous high-resolution SSI, we recommend decreasing the temporal resolution of surface measurements to 30–40 min and decreasing the spatial resolution of satellite-based SSI to an area larger than 5 km × 5 km to reduce the validation uncertainty.

In spite of this, the impact of the 3D effect of clouds is still difficult to eliminate completely. An extreme case is when a cloud only exists in the solar-to-surface path or in the surface-to-satellite path as illustrated in Fig. 5. In this scenario, a pair of opposite atmospheric conditions (clear and cloudy) is observed by satellites and by surface sites, respectively. The validation result will be severely contaminated. Therefore, some studies have suggested that extreme cases should be excluded when the difference between an instantaneous retrieval and a surface observation is larger than the triple standard deviation of their difference (Pinker et al., 2009; Qin et al., 2015; Wang and Pinker, 2009).

Note that the validation uncertainty due to the 3D effect of clouds rapidly decreases as the timescale of a satellite product increases. When the timescales of satellite products are ≥3 h, we generally ignore the impacts of the 3D effect of clouds on validations (Huang et al., 2016a). Therefore, for 3-hour, monthly, or yearly high-resolution SSI products, the validation strategy of a straight comparison does not need any adjustments.

4.2. Validations of the coarse-resolution gridded SSI

The term "grid" in coarse-resolution gridded products refers exclusively to larger geographic latitude-longitude grids that are generally ≥0.25° (global SSI products are usually produced at these spatial scales). As spatial scales increase, point-specific surface measurements become increasingly inadequate to characterize and represent grid-level surroundings (Li et al., 2013). The uncertainty due to the spatial representativeness error thereby becomes more important. Here, the spatial representativeness error is defined as the sampling error originating from the different spatial scales between in-situ measurements and satellite products (Jin et al., 2017; Liu and Li, 2017).

Though not considered in most operational validations (Pinker et al., 2005; Yang et al., 2008; Zhang et al., 2013; Zhang et al., 2015), the inadequate spatial representativeness of surface measurements has long been realized. When using GEBA measurements to validate two monthly satellite-based products, Li et al. (1995) found that if multiple GEBA sites within a grid cell were simultaneously employed, the discrepancy between products and measurements would significantly drop to ~5 W m^{-2}, versus > 20 W m^{-2} obtained using single site. Li et al. (2005) used high-resolution kilometer-scale SSI retrievals to quantify the representativeness error of a single surface site within a given grid domain. Their study revealed that the spatial representativeness error (uncertainty) is not only contingent upon the spatial scale of the validated products, but also their temporal cycles. Inspired by Li et al. (2005), Hakuba et al. (2013) studied the spatial representativeness of 143 surface stations in Europe and demonstrated a maximal annual RMAD (relative mean absolute deviation) of up to 10% and an average annual RMAD of ~1.6% for a standard grid of 1°. Using a similar approach, Hakuba et al. (2014) expanded their study to the entire Meteosat disk (the zone between 70°W to 70° E and 70°S to 70°N). Schwarz et al. (2018) presented a near-global investigation on the representativeness of SSI point observations.

When using high-resolution satellite products to investigate the subgrid spatial variability and the spatial representativeness, the variability of SSI within these products is in fact omitted. A more comprehensive investigation was conducted by Huang et al. (2016a) in which representativeness errors were calculated by combining high-resolution satellite products and a dense matrix of surface observations. They found that when doing a validation using a single site's measurements, the resulting uncertainty is much larger than the accuracy criteria proposed by many applications (e.g., climate change monitoring), and significant enough to undermine some validation conclusions we have made.

Generally, the spatial representativeness error decreases rapidly as the timescale increases up to one day and levels off to a relatively small value (Li et al., 2005). On a monthly timescale, Hakuba et al. (2014) and Schwarz et al. (2018) both found that the majority of stations are representative within the in-situ measurement accuracy except near coasts, mountains, and in the tropics. But on shorter timescales (≤ one day) spatial representativeness errors may be considerably large and significantly affect the results of validations. Huang et al. (2016a), therefore, proposed a cross-validation strategy, namely using a well-validated high-resolution SSI product as a reference to assess the gridded product that needs to be validated. This strategy is also known as a hierarchical validation strategy. High-resolution SSI product is first validated and calibrated using in-situ measurements to remove any potential systematic bias. The resulting unbiased high-resolution SSI is then used to evaluate the gridded product.

In short, SSI gridded products can be assessed using single-site measurements, but considerable uncertainties may be incurred. The cross-validation strategy likely provides a more appropriate alternative for validating SSI gridded products.

5. Products and accuracies

As mentioned in Section 4, there are two groups of SSI products: high-resolution kilometer-scale products and coarse-resolution gridded products. The following describes their respective statuses.

5.1. High-resolution SSI products and accuracies

To date, mature high-resolution SSI datasets with global and multi-year coverage are still rare. High-resolution kilometer-scale products are mainly produced over specific regions like Europe, North America, and China, or are produced on the basis of one specific satellite (or sensor) like the Geostationary Operational Environmental Satellite (GOES), SEVIRI, MTSAT, etc. (Bisht and Bras, 2010; Bisht et al., 2005; Deneke et al., 2008; Forman and Margulis, 2009; Hollmann et al., 2006; Huang et al., 2016b; Huang et al., 2012; Huang et al., 2011; Lu et al., 2010; Mueller et al., 2004; Mueller et al., 2009; Pinker et al., 2003; Tang et al., 2016; Wang and Pinker, 2009).

From these studies, different satellite missions/sensors have been employed to generate SSI products of varying uncertainties that are generally acceptable. Over mid-latitude regions, the RMSE of instantaneous retrievals are frequently within 50 W m^{-2} (≤10% of the mean SSI) for clear skies, while for all skies, it may range from 60 W m^{-2} to 140 W m^{-2} (~15–30% of the mean SSI) depending on the local cloud climatology. The quality of hourly SSI is frequently slightly better than that of instantaneous SSI (Deneke et al., 2008; Huang et al., 2016b). The accuracy substantially improves as the timescale increases up to one day or more. For daily SSI, the typical RMSE is ~35 W m^{-2} (~10% of the mean SSI), and for monthly SSI, some studies have reported RMSEs < 10 W m^{-2} (≤5% of the mean SSI; Mueller et al., 2009; Qin et al., 2011).

In general, most physical algorithms tend to overestimate SSI over snow-free surfaces and underestimate SSI over snow-covered surfaces (Huang et al., 2016b; Li et al., 2007; Pinker et al., 2007). Particularly for the estimation of instantaneous SSI under cloudy-sky conditions, many studies have demonstrated a systematic overestimation over snow-free surfaces (Huang et al., 2013; Liang et al., 2006; Lu et al., 2010; Zhang et al., 2014). A plausible explanation is the satellite signal saturation for very thick clouds that results in underestimated COD (Huang et al., 2016b; Platnick et al., 2015). The difficulty in completely identifying intermittent snow-cover periods causes the underestimation over snow-covered surfaces. If snow under clouds goes undetected, COD is overestimated, and SSI is underestimated (Pinker et al., 2003).

Although a well-established global kilometer-scale SSI product is not available yet, regional kilometer-scale products covering almost all of the world's middle and low latitude areas, including Europe, Africa, East Asia, and North America, are available. In recent years, many scholars have pointed out the necessity and demand to produce high spatiotemporal resolution SSI over the globe (Huang et al., 2013; Yang et al., 2008; Zhang et al., 2014). In support of the Global LAnd Surface Satellite (GLASS) project (Liang et al., 2014), Zhang et al. (2014) generated a set of experimental, 5-km resolution, globe-covering SSI products from 2000 to 2017 by combining multiple polar-orbiting and geostationary data (http://glass-product.bnu.edu.cn/). During the preparation of our paper, MODIS global 5-km downward shortwave radiation and PAR (MCD18) was also released (https://lpdaac.usgs.gov/). We have no reason to doubt that there will be more and better products appearing in the near future.

Moreover, there are a few commercial high-resolution SSI datasets with near-global coverage for solar energy assessment and operation.

Table 3
Summary of current global gridded SSI products and the algorithms adopted.

Products	Resolutions	Coverage	Methods	Main inputs	Website
GEWEX SRB	• Spatial: 1° • Temporal: 3-hour; daily; monthly	1983.7–2007.12	• Primary algorithm Modified LUT method described originally by Pinker and Laszlo (1992). • Langley Parameterized SW Algorithms (LPSA) Developed according to the parameterizations of Gupta et al. (2001), and designated as quality-check.	• ISCCP DX radiance • GEOS-4 reanalysis atmosphere • TOMS ozone	https://gewex-srb.larc.nasa.gov/index.php
ISCCP FD	• Spatial: 2.5° • Temporal: 3-hour	1983.7–2009.12	• GISS GCM radiation model NASA GISS climate Global Circulation Model (GCM) radiative transfer code described by Hansen et al. (2002) and Oinas et al. (2001).	• ISCCP-D1/ISCCP-D2 gridded cloud • TOMS ozone • TOVS atmosphere • GISS climatological aerosols	https://isccp.giss.nasa.gov/projects/flux.html
CERES level 2-3B products	• Spatial: 1° • Temporal: Instantaneous; daily; monthly	2000.3–2013.3	• SSF[a] level 2 product Parameterization of Li et al. (1993b) and LPSA algorithms (Gupta et al., 2001). • SYN1deg level 3 product Delta-two stream radiation transfer code • EBAF[b] level 3B product Adjust surface flux using CERES-derived TOA flux as constraints. The tuning algorithm is described by Kato et al. (2013).	• CERES TOA observations • CERES geostationary cloud properties • GEOS-4/5 reanalysis atmosphere • MODIS clouds and aerosols products	https://ceres.larc.nasa.gov/index.php
UMD SRB	• Spatial: 0.5° • Temporal: 3-hour; daily; monthly	1983.7–2007.6	• Updated LUT method The LUT algorithm originally developed by Pinker and Laszlo (1992) and updated by Ma and Pinker (2012).	• ISCCP DX radiance • TOVS[c] atmosphere • Other auxiliary data	http://www.atmos.umd.edu/~srb/index.html
CM SAF CLARA	• Spatial:0.25° • Temporal: Daily; monthly	1982.1–2015.12	• LUT based eigenvector hybrid method More effective LUT method proposed by Mueller et al. (2009), which is also based on the LUT method of Pinker and Laszlo (1992).	• AVHRR GAC radiance • ERA-Interim reanalysis atmosphere • GADS/OPAC[d] aerosol climatology	https://wui.cmsaf.eu/safira/action/viewHome?

[a] SSF: Surface Fluxes and Clouds.
[b] EBAF: Energy Balanced and Filled.
[c] TOVS: TIROS Operational Vertical Sounder.
[d] GADS/OPAC: Global Aerosol Data Set/Optical Properties of Aerosols and Clouds.

For example, the SolarGIS coverage extends 60°N to 50°S (https://solargis.com/). Given their high quality and up to real time update, they have played an important role in the solar energy industry today.

5.2. Coarse-resolution gridded SSI products and accuracies

Unlike the kilometer-scale products, there are already several global, coarse-resolution, gridded SSI products that have been released since the 1990s. Common ones include the GEWEX SRB products, the ISCCP Flux dataset (FD) products, the CERES products, the UMD SRB products, and the CM SAF products. Table 3 summarizes these products and the algorithms involved. Note that many of the products focus not only on SSI but also on other radiation budget components both at the surface and the TOA. Therefore, many algorithms listed in the table are not designed specifically for the estimation of SSI.

A quantitative description of the accuracy of each dataset is intentionally omitted here because it varies from study to study, region to region, and version to version, depending on the specific latitude, aerosol climatology, and cloud climatology. But roughly speaking on a monthly timescale typical RMSEs of these global products range from 20 $W m^{-2}$ to 35 $W m^{-2}$, and overall the CERES-EBAF product may be better than other products (Pinker et al., 2005; Zhang et al., 2013; Zhang et al., 2014). On a daily timescale the RMSE fluctuates dramatically, but values between 30 and 40 $W m^{-2}$ are the most common (Zhang et al., 2013). In general accuracies of these products worsen and discrepancies between different products strengthen in some remote regions. For example, over the Arctic, Riihela et al. (2017) found that the RMSE of GEWEX SRB daily products reached as high as 60.4 $W m^{-2}$ in summer and satellite-based estimates are not homogeneous. CERES daily products are more accurate than the other daily products. Over the Tibetan Plateau, on monthly timescale Yang et al. (2006a) reported that the RMSEs of ISCCP FD and GEWEX SRB products are 17 $W m^{-2}$ and 50 $W m^{-2}$, respectively. The ISCCP FD products clearly outperform GEWEX SRB products. However, on a daily timescale RMSEs are, respectively, 34 $W m^{-2}$ and 39 $W m^{-2}$. In this case, the ISCCP FD products are slightly worse than GEWEX SRB products (Yang et al., 2008). Therefore, further efforts are necessary to investigate the differences between different products over these areas. Of course, as mentioned before, RMSE in here cannot be attributed to the accuracy problem of satellite products completely because bulk of it may be due to large sampling errors in surface point-specific measurements compared with gridded satellite products (Li et al., 1995).

Similar to kilometer-scale products, there is also an overestimation of SSI over snow-free surfaces as a whole in gridded products, an improving tendency in accuracy with decreasing temporal resolution, and a drop in quality during the winter and spring seasons because of the influence of intermittent snow cover. After an in-depth assessment of four widely-used monthly gridded products (CERES-EBAF, GEWEX-SRB, UMD-SRB, and ISCCP-FD) using 1152 globally distributed GEBA stations and 99 China Meteorological Administration (CMA) stations in China, Zhang et al. (2015) concluded that SSI is overall overestimated by ~10 $W m^{-2}$. Over 80% of the CMA stations show positive biases, and only one clear negative bias is seen at the station on the Tibetan Plateau (see Fig. 3 in their paper). Such a conclusion is consistent with other studies (Wu and Fu, 2011; Xia et al., 2006), which suggests that these global products likely systematically overestimate SSI over China except for the Tibetan Plateau. Owing to the highly variable terrain and more frequent snow cover, satellite products for the Tibetan Plateau are usually less accurate than for other regions (Yang et al., 2006a; Yang et al., 2008).

While retrievals of SSI are far better than the retrievals of other variables such as evapotranspiration, leaf area index, and surface soil moisture, this does not mean that its accuracy level can readily meet the demand of a particular study or application in need of SSI. Let us look again at the WMO accuracy criteria listed in Table 1. Even the basic "threshold" grades are a challenge for current SSI products to meet. As early as the 1980s, the World Climate Research Program had set the goal of deriving a global monthly climatology of radiative fluxes with an accuracy of 10 $W m^{-2}$ (RMSE) over a spatial resolution of 250 km (~2.5°; Suttles and Ohring, 1986). Until now whether this accuracy goal has been reached is still unclear. The previous studies (Pinker et al., 1995) reported a monthly accuracy of ~20 $W m^{-2}$ on a global scale, and recent products appear to have improved this accuracy (Ma and Pinker, 2012). Anyway, satellite products still have a long way to go to meet the demands proposed of many applications. Lowering the uncertainties in the satellite-based estimation of SSI is still crucial in the next decade.

6. Current problems and future perspectives

Although current SSI-related studies have become increasingly quantitative and sophisticated, there has not been a substantial improvement in product quality due to various practical difficulties and problems. Some key difficulties and problems are:

(1) The impact of 3D effect of clouds on the estimation of high-resolution SSI, especially instantaneous SSI, is very difficult to eliminate. In theory, current satellite-based estimations are all conducted under the assumption of an independent pixel approximation (IPA), but strictly speaking, the IPA assumption only makes sense for lower spatial resolution retrievals. As the spatial resolution increases to several kilometers, the area affected by spatially inhomogeneous clouds (generally ≥25 km) is much larger than the footprint of an individual pixel. Therefore, the IPA is no longer justified (Wyser et al., 2002). This means that the theoretical basis of the retrievals would be difficult to uphold when estimating high-resolution SSI. Despite the large uncertainty caused by the 3D variability of clouds, retrieval algorithms are unable to tackle the problem. This uncertainty is perhaps the largest error source for instantaneous SSI retrievals (Wyser et al., 2005).

(2) The complexity of clouds is another intractable barrier for the improvement of satellite-based SSI products. In nature multilayer clouds are not uncommon (Chang and Li, 2005; Desmons et al., 2017), and so are mixed-phase clouds (Wood, 2008). Both of these issues affect the estimation of SSI significantly, but are not easy to address within the scope of passive optical remote sensing (Platnick et al., 2003; Platnick et al., 2017). These complex issues are so difficult to resolve that the incurring uncertainties can readily overshadow those gained through the improvement of a retrieval algorithm. For example, in principle, ice clouds and water clouds have distinct optical properties, and distinguishing between them in algorithms would improve estimation of SSI. However, Deneke et al. (2005) and Huang et al. (2016b) have both shown that the SSI accuracy cannot be significantly improved even if the ISCCP thermal infrared threshold algorithm is used to distinguish them (Rossow and Schiffer, 1999).

(3) Reliable aerosol information also constrains the accuracy of estimates of SSI under clear-sky conditions. As the only means to obtain regional or global aerosol distributions (King et al., 1999; Lee et al., 2009), aerosol retrievals over land surface are still fraught with challenges as discussed in Section 2.2. Because there are no high-quality satellite-based aerosol products, auxiliary aerosol climatology datasets are often used instead to estimate SSI in many operational algorithms. However, the accuracies of most aerosol climatology datasets are considerably low in many regions (Li et al., 2009). An integrated aerosol product that merges multi-source aerosol data including various satellite-based products, ground-based observations, and some good climatology datasets needs to be urgently developed.

(4) Globally representative cloud and aerosol optical models, especially ice cloud models and aerosol models over some regions are still subjects of debate (Baum et al., 2011; Deneke et al., 2005; Xin et al.,

2011; Yang et al., 2013; Zhang et al., 2002). As a prerequisite of the remote sensing of clouds and aerosols, this not only affects the retrievals themselves, but also SSI estimates. For instance, Huang et al. (2011) and Wang et al. (2014) have shown that use of an improper aerosol model (characterized by the SSA and the asymmetry factor) in a region undergoing rapid industrialization and urbanization may be a major reason for the SSI overestimation in East China (aerosol absorption is underestimated). The acquisition of representative cloud and aerosol optical models depends on ground-based or airborne measurements of clouds and aerosols. With the establishment of more observation networks and the release of more measured data, there may be a substantial advance in this respect in the foreseeable future.

(5) Snow/Ice cover may affect the estimation of SSI significantly. Clouds and snow have similar reflective optical characteristics in many spectral regions. While it is possible to identify clouds over bright snow/ice surface (Li and Leighton, 1991), retrievals of cloud optical depths over such surfaces are subject to large uncertainties (Platnick et al., 2015; Platnick et al., 2001; Platnick et al., 2017). It is even more challenging over short-lived snow or ice (Pinker et al., 2007). As discussed in Section 5.1, this may result in a lower accuracy in satellite estimation of SSI (Huang et al., 2016b; Li et al., 2007).

(6) Sparse spectral channels of previous geostationary satellites as well as small number of overpasses of polar-orbiting satellite systems limits the more quantitative acquisition of historical SSI (Deneke et al., 2008). The previous generation of geostationary satellites usually had only one channel in the reflection part of the solar spectrum. This made the detection of thin clouds such as cirrus problematic (Ricciardelli et al., 2008), and AOD retrieval difficult to implement. Therefore, for historic geostationary data, some studies proposed combining polar-orbiting satellite data to estimate the surface radiation budget (Huang et al., 2011; Tang et al., 2016).

(7) When creating long-term, continuous, and consistent databases to study the long-term trends of SSI, sensor-related issues may undermine our efforts (Blanc et al., 2011; Ma and Pinker, 2012). Besides recalibration due to sensor degradation, other issues include possible slight discrepancies in spectral response functions among sensors, sampling changes in space and time during different periods, changes of numbers of sensor channels, etc. These issues are not new and were noted earlier on by Schiffer and Rossow (1985). For more detailed discussions, we refer the interested readers to Whitlock et al. (1995) and Blanc et al. (2011).

The above are just a few difficulties or problems facing the remote sensing of SSI from the satellite meteorology perspective. Actual difficulties may be more than those, e.g., the effect of topography in complex mountain areas (Gu et al., 2012; Liou et al., 2013; Yang et al., 2008). Further improvements are expected in the development of new methods or techniques to address these problems (Li et al., 2007), specially quantitative assessments and eliminations of 3D effect of clouds and proper treatments of aerosol influences. The 3D effect of clouds can significantly affect the high temporal resolution retrievals of SSI (≤ 3 h), and is always the largest error source of resulting SSI products. Several studies in recent years have already tried to address this problem by combining numerical weather model and 3D radiative transfer theory developed for light propagation in the real atmosphere (Gu et al., 2012; Liou et al., 2013). But these studies are still in the experimental stage. A general solution on how to tackle such a problem has not been proposed. Until the 3D effect of clouds is eliminated, it is infeasible to substantially improve SSI accuracy at a high temporal resolution.

Meanwhile, not only aerosol loading but also aerosol optical properties will affect the long-term estimation of SSI. The SSA of aerosol typically ranges from 0.96 for areas with a pristine atmosphere, to 0.93 for a typical rural area, to 0.86 for a typical urban area, and to 0.67 for a highly polluted area (Li et al., 2009). This results in large uncertainties in the estimation of aerosol absorption that is especially important for it determines the amount of solar radiation absorbed in the atmosphere. The worst happens if absorbing aerosol is mixed with clouds that can drastically lower the TOA reflection and lead to a large overestimation of SSI (Li et al., 2014). In the tropical Africa and Amazon regions during the biomass burning season an overestimation of up to 100 Wm^{-2} on a monthly scale may be seen (Li, 1998). The value of aerosol SSA is very difficult to acquire over large scales, and may fluctuate dramatically because it is largely affected by the industrialization, and human activities. For example, at an urban center and the nearby surrounding, there may be two distinct values even if they are not too far. Solutions to aerosol-related problems need the collective effort of ground-based observation and satellite remote sensing. Currently a global network, Aerosol Robotic NETwork (AERONET), had been established by NASA and other collaborators. With more ground-based observations and the development of new satellite remote sensing techniques, a better solution may be seen in the near future.

The progress of satellite-based SSI also depends on advancements in satellite sensor technology. Of the recently new launched satellite sensors, particularly noteworthy are various multispectral sensors onboard the new generation of geostationary satellites and the Earth Polychromatic Imaging Camera (EPIC) onboard the Deep Space Climate Observatory (DSCOVR) satellite. The first modern generation of geostationary satellites is Meteosat-8, which was launched by the EUMETSAT in 2002. As the Meteosat-8 satellite's main payload, the SEVIRI, has up to 12 spectral channels (4 visible/near-infrared channels and 8 infrared channels) and has shown a stronger ability to identify cloud properties, composition, and dynamics (Henken et al., 2011; Stengel et al., 2014). Accordingly a better estimation of high-resolution SSI is expected (Deneke et al., 2008). Following in the footsteps of the Meteosat-8, Himawari-8, GOES-R, and FengYun-4 new generation of geostationary satellites were launched in succession from 2014 to 2016 by Japan, the U.S., and China, respectively. The new optical imaging radiometers carried by these satellites have not only a higher spectral resolution (up to 16 channels) but also higher spatial and temporal resolutions. This provides a new opportunity for estimating regional and global SSI.

Different from all previous satellites, the DSCOVR satellite orbits a special space location called the Lagrange point 1 (or simply L1), which is one of the neutral gravity points between the Sun and Earth. From this location, the satellite can keep its onboard Earth-observing sensor viewing the earth in the direction of the sun at all times, i.e., continuously viewing the sunlit side of the earth. Such a unique observation mode (see Fig. 6) ensures that the atmospheric column that determines the surface incident solar irradiance is the same one as observed by the satellite. Thus 3D radiative effects due to inhomogeneous atmospheric constituents can be substantially reduced and the quality of SSI is expected to improve. DSCOVR-EPIC will provide a unique vantage point for studies of high-resolution SSI. However, its current resolution is only 25 km.

Since reliable ground observation is chiefly available in the populated middle and low latitudes, satellite-based estimates are more needed in remote regions like the Arctic, the Tibetan Plateau, and the Antarctic etc. These regions are research hotspots in earth science. But as mentioned before, current satellite products still have a large uncertainty. Studies on how to improve the SSI accuracy in these regions should be of scientific interest in the future (Riihela et al., 2017; Yang et al., 2008). Over these decades, in fact there are already many SSI products available over most regions. Perhaps developing various data fusion methods to assimilate the merits of these products and subsequently reduce the uncertainties is also promising. For example, through integrating surface observation data, satellite products as well as reanalysis datasets, Shi and Liang (2013a) generated a fusion dataset using the multiple linear regression method, which demonstrate a

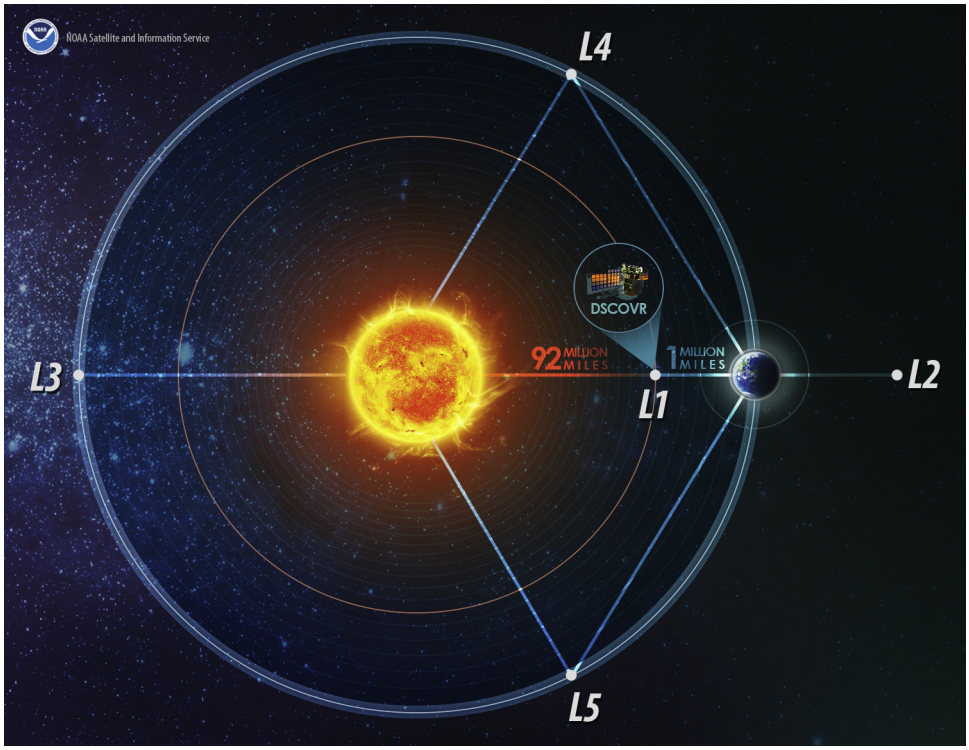

Fig. 6. Illustration of the unique observation mode of the DSCOVR-EPIC.
(Taken from https://www.nesdis.noaa.gov/content/dscovr-deep-space-climate-observatory.)

better quality over Tibetan Plateau (Shi and Liang, 2013b). Forman and Margulis (2010) introduced the Ensemble Kalman Filter to assimilate satellite products with different resolutions and sources. Compared with previous studies, not only the optimal estimate of SSI is given, but also its uncertainty. This provides an alternative mean of understanding and characterization of the variability in SSI.

In short, estimating SSI from satellites has been a "classical" remote sensing problem that has been tackled for nearly half a century. While substantial progresses have been made in improving its retrieval accuracy that is better than many other geophysical quantities (in terms of relative error), daunting challenges still confront us. It will continue to be a major subject of remote sensing in the future.

Acknowledgments

This work was supported by the Strategic Priority Research Program of the Chinese Academy of Sciences (grant: XDA20100104), the Natural Science Foundation of China (grant: 41571358), and the Youth Innovation Promotion Association, Chinese Academy of Sciences. Z. Li is supported by the State Key Laboratory of Remote Sensing Science, jointly sponsored by Beijing Normal University and Institute of Remote Sensing and Digital Earth of Chinese Academy of Sciences, Beijing 100875, China.

Appendix A. Terminology and symbols

AERONET	AERONET
AOD	Aerosol Optical Depth
AVHRR	Advanced Very High Resolution Radiometer
CERES	Clouds and the Earth's Radiant Energy System
CLARA	CLoud, Albedo and RAdiation dataset, AVHRR-based
CM SAF	Satellite Application Facility on Climate Monitoring
CMA	China Meteorological Administration
COD	Cloud Optical Depth
DSCOVR	Deep Space Climate Observatory
EBAF	Energy Balanced and Filled
EPIC	Earth Polychromatic Imaging Camera
ERBE	Earth Radiation Budget Experiment
EUMETSAT	European Organization for the Exploitation of Meteorological Satellites
FD	Flux Data
GADS/OPAC	Global Aerosol Data Set/Optical Properties of Aerosols and Clouds
GCM	General Circulation Model
GEBA	Global Energy Balance Archive
GEOS	Goddard Earth Observing System
GEWEX	Global Energy and Water cycle Exchanges
GISS	Goddard Institute for Space Studies
GMS	Geostationary Meteorological Satellite
GOES-R	Geostationary Operational Environmental Satellite-R Series
GSFC	Goddard Space Flight Center
IPA	Independent Pixel Approximation
ISCCP	International Satellite Cloud Climatology Project
LUT	Look-up Table
MODIS	Moderate Resolution Imaging Spectroradiometer
MODTRAN	MODerate resolution atmospheric TRANsmission
MTSAT	Multifunctional Transport Satellites
NASA	National Aeronautics and Space Administration
NSSI	Net Surface Solar Radiation
PAR	Photosynthetically Active Radiation
RMAD	Relative Mean Absolute Deviation
RMSE	Root Mean Square Error
RTM	Radiative Transfer Model
SEVIRI	Spinning Enhanced Visible and Infrared Imager
SRB	Surface Radiation Budget
SSA	Single Scattering Albedo
SSF	Surface Fluxes and Clouds
SSI	Surface Solar Irradiance
SSRB	Solar Surface Radiation Budget
TIROS	Television Infrared Observation Satellites

TOA Top Of the Atmosphere
TOMS Total Ozone Mapping Spectrometer
TOVS TIROS Operational Vertical Sounder
UMD University of Maryland
WMO World Meteorological Organization
WMO OSCAR WMO Observing System Capability Analysis and Review Tool

References

Aguiar, L.M., Pereira, B., David, M., Diaz, F., Lauret, P., 2015. Use of satellite data to improve solar radiation forecasting with Bayesian Artificial Neural Networks. Sol. Energy 122, 1309–1324.
Akarslan, E., Hocaoglu, F.O., 2016. A novel adaptive approach for hourly solar radiation forecasting. Renew. Energy 87, 628–633.
Akarslan, E., Hocaoglu, F.O., Edizkan, R., 2014. A novel M-D (multi-dimensional) linear prediction filter approach for hourly solar radiation forecasting. Energy 73, 978–986.
Baum, B.A., Yang, P., Heymsfield, A.J., Schmitt, C.G., Xie, Y., Bansemer, A., Hu, Y.X., Zhang, Z.B., 2011. Improvements in shortwave bulk scattering and absorption models for the remote sensing of ice clouds. J. Appl. Meteorol. Climatol. 50, 1037–1056.
Beyer, H.G., Costanzo, C., Heinemann, D., 1996. Modifications of the Heliosat procedure for irradiance estimates from satellite images. Sol. Energy 56, 207–212.
Bhartia, P.K., McPeters, R.D., Mateer, C.L., Flynn, L.E., Wellemeyer, C., 1996. Algorithm for the estimation of vertical ozone profiles from the backscattered ultraviolet technique. J. Geophys. Res.-Atmos. 101, 18793–18806.
Bisht, G., Bras, R.L., 2010. Estimation of net radiation from the MODIS data under all sky conditions: Southern Great Plains case study. Remote Sens. Environ. 114, 1522–1534.
Bisht, G., Venturini, V., Islam, S., Jiang, L., 2005. Estimation of the net radiation using MODIS (Moderate Resolution Imaging Spectroradiometer) data for clear sky days. Remote Sens. Environ. 97, 52–67.
Blanc, P., Gschwind, B., Lefevre, M., Wald, L., 2011. The HelioClim Project: surface solar irradiance data for climate applications. Remote Sens. 3, 343–361.
Briegleb, B.P., 1992. Delta-Eddington approximation for solar-radiation in the Ncar community climate model. J. Geophys. Res.-Atmos. 97, 7603–7612.
Cano, D., Monget, J.M., Albuisson, M., Guillard, H., Regas, N., Wald, L., 1986. A method for the determination of the global solar-radiation from meteorological satellite data. Sol. Energy 37, 31–39.
Cess, R.D., Vulis, I.L., 1989. Inferring surface solar absorption from broadband satellite measurements. J. Clim. 2, 974–985.
Cess, R.D., Zhang, M.H., Minnis, P., Corsetti, L., Dutton, E.G., Forgan, B.W., Garber, D.P., Gates, W.L., Hack, J.J., Harrison, E.F., Jing, X., Kiehl, J.T., Long, C.N., Morcrette, J.J., Potter, G.L., Ramanathan, V., Subasilar, B., Whitlock, C.H., Young, D.F., Zhou, Y., 1995. Absorption of solar-radiation by clouds - observations versus models. Science 267, 496–499.
Chang, F.L., Li, Z.Q., 2005. A near-global climatology of single-layer and overlapped clouds and their optical properties retrieved from Terra/MODIS data using a new algorithm. J. Clim. 18, 4752–4771.
Chou, M.D., 1991. The derivation of cloud parameters from satellite-measured radiances for use in surface radiation calculations. J. Atmos. Sci. 48, 1549–1559.
Ciren, P.B., Li, Z.Q., 2003. Long-term global earth surface ultraviolet radiation exposure derived from ISCCP and TOMS satellite measurements. Agric. For. Meteorol. 120, 51–68.
Darnell, W.L., Staylor, W.F., Gupta, S.K., Denn, F.M., 1988. Estimation of surface insolation using sun-synchronous satellite data. J. Clim. 1, 820–835.
Decker, M., Brunke, M.A., Wang, Z., Sakaguchi, K., Zeng, X.B., Bosilovich, M.G., 2012. Evaluation of the reanalysis products from GSFC, NCEP, and ECMWF using flux tower observations. J. Clim. 25, 1916–1944.
Deneke, H., Feijt, A., van Lammeren, A., Simmer, C., 2005. Validation of a physical retrieval scheme of solar surface irradiances from narrowband satellite radiances. J. Appl. Meteorol. 44, 1453–1466.
Deneke, H.M., Feijt, A.J., Roebeling, R.A., 2008. Estimating surface solar irradiance from METEOSAT SEVIRI-derived cloud properties. Remote Sens. Environ. 112, 3131–3141.
Deneke, H.M., Knap, W.H., Simmer, C., 2009. Multiresolution analysis of the temporal variance and correlation of transmittance and reflectance of an atmospheric column. J. Geophys. Res.-Atmos. 114.
Desmons, M., Ferlay, N., Parol, F., Riedi, J., Thieuleux, F., 2017. A global multilayer cloud identification with POLDER/PARASOL. J. Appl. Meteorol. Climatol. 56, 1121–1139.
Emde, C., Buras-Schnell, R., Kylling, A., Mayer, B., Gasteiger, J., Hamann, U., Kylling, J., Richter, B., Pause, C., Dowling, T., Bugliaro, L., 2016. The libRadtran software package for radiative transfer calculations (version 2.0.1). Geosci. Model Dev. 9, 1647–1672.
Forman, B.A., Margulis, S.A., 2009. High-resolution satellite-based cloud-coupled estimates of total downwelling surface radiation for hydrologic modelling applications. Hydrol. Earth Syst. Sci. 13, 969–986.
Forman, B.A., Margulis, S.A., 2010. Assimilation of multiresolution radiation products into a downwelling surface radiation model: 2. Posterior ensemble implementation. J. Geophys. Res.-Atmos. 115.
Fritz, S., Rao, P.K., Weinstein, M., 1964. Satellite measurements of reflected solar energy and the energy received at the ground. J. Atmos. Sci. 21, 141–151.
Gao, B.C., Kaufman, Y.J., 2003. Water vapor retrievals using moderate resolution imaging spectroradiometer (MODIS) near-infrared channels. J. Geophys. Res.-Atmos. 108.
Gautier, C., Diak, G., Masse, S., 1980. A simple physical model to estimate incident solar-radiation at the surface from Goes satellite data. J. Appl. Meteorol. 19, 1005–1012.
Gu, Y., Liou, K.N., Lee, W.L., Leung, L.R., 2012. Simulating 3-D radiative transfer effects over the Sierra Nevada Mountains using WRF. Atmos. Chem. Phys. 12, 9965–9976.
Gueymard, C.A., 2003a. Direct solar transmittance and irradiance predictions with broadband models. Part I: detailed theoretical performance assessment. Sol. Energy 74, 355–379.
Gueymard, C.A., 2003b. Direct solar transmittance and irradiance predictions with broadband models. Part II: validation with high-quality measurements. Sol. Energy 74, 381–395.
Gupta, S.K., Kratz, D.P., Stackhouse, P.W., Wilber, A.C., 2001. The Langley Parameterized Shortwave Algorithm (LPSA) for Surface Radiation Budget Studies (Version 1.0).
Hakuba, M.Z., Folini, D., Sanchez-Lorenzo, A., Wild, M., 2013. Spatial representativeness of ground-based solar radiation measurements. J. Geophys. Res.-Atmos. 118, 8585–8597.
Hakuba, M.Z., Folini, D., Sanchez-Lorenzo, A., Wild, M., 2014. Spatial representativeness of ground-based solar radiation measurements-extension to the full Meteosat disk. J. Geophys. Res.-Atmos. 119, 11760–11771.
Hammer, A., Heinemann, D., Hoyer, C., Kuhlemann, R., Lorenz, E., Muller, R., Beyer, H.G., 2003. Solar energy assessment using remote sensing technologies. Remote Sens. Environ. 86, 423–432.
Hansen, J., Sato, M., Nazarenko, L., Ruedy, R., Lacis, A., Koch, D., Tegen, I., Hall, T., Shindell, D., Santer, B., Stone, P., Novakov, T., Thomason, L., Wang, R., Wang, Y., Jacob, D., Hollandsworth, S., Bishop, L., Logan, J., Thompson, A., Stolarski, R., Lean, J., Willson, R., Levitus, S., Antonov, J., Rayner, N., Parker, D., Christy, J., 2002. Climate forcings in Goddard Institute for Space Studies SI2000 simulations. J. Geophys. Res.-Atmos. 107.
Henken, C.C., Schmeits, M.J., Deneke, H., Roebeling, R.A., 2011. Using MSG-SEVIRI cloud physical properties and weather radar observations for the detection of Cb/TCu clouds. J. Appl. Meteorol. Climatol. 50, 1587–1600.
Hollmann, R., Mueller, R.W., Gratzki, A., 2006. CM-SAF surface radiation budget: first results with AVHRR data. Atmospheric Remote Sensing: Earth's Surface, Troposphere, Stratosphere and Mesosphere - Ii 37, 2166–2171.
Holz, R.E., Platnick, S., Meyer, K., Vaughan, M., Heidinger, A., Yang, P., Wind, G., Dutcher, S., Ackerman, S., Amarasinghe, N., Nagle, F., Wang, C.X., 2016. Resolving ice cloud optical thickness biases between CALIOP and MODIS using infrared retrievals. Atmos. Chem. Phys. 16, 5075–5090.
Hsu, N.C., Jeong, M.J., Bettenhausen, C., Sayer, A.M., Hansell, R., Seftor, C.S., Huang, J., Tsay, S.C., 2013. Enhanced deep blue aerosol retrieval algorithm: the second generation. J. Geophys. Res.-Atmos. 118, 9296–9315.
Huang, G.H., Ma, M.G., Liang, S.L., Liu, S.M., Li, X., 2011. A LUT-based approach to estimate surface solar irradiance by combining MODIS and MTSAT data. J. Geophys. Res.-Atmos. 116.
Huang, G.H., Liu, S.M., Liang, S.L., 2012. Estimation of net surface shortwave radiation from MODIS data. Int. J. Remote Sens. 33, 804–825.
Huang, G.H., Wang, W.Z., Zhang, X.T., Liang, S.L., Liu, S.M., Zhao, T.B., Feng, J.M., Ma, Z.G., 2013. Preliminary validation of GLASS-DSSR products using surface measurements collected in arid and semi-arid regions of China. Int. J. Digital Earth 6, 50–68.
Huang, G.H., Huang, C.L., Li, Z.Q., Chen, H., 2015. Development and validation of a robust algorithm for retrieving aerosol optical depth over land from MODIS data. Ieee Journal of Selected Topics in Applied Earth Observations and Remote Sensing 8, 1152–1166.
Huang, G.H., Li, X., Huang, C.L., Liu, S.M., Ma, Y.F., Chen, H., 2016a. Representativeness errors of point-scale ground-based solar radiation measurements in the validation of remote sensing products. Remote Sens. Environ. 181, 198–206.
Huang, G.H., Li, X., Ma, M.G., Li, H.Y., Huang, C.L., 2016b. High resolution surface radiation products for studies of regional energy, hydrologic and ecological processes over Heihe river basin, northwest China. Agric. For. Meteorol. 230, 67–78.
Huang, G.H., Liang, S.L., Lu, N., Ma, M.G., Wang, D.D., 2018. Toward a broadband parameterization scheme for estimating surface solar irradiance: development and preliminary results on MODIS products. J. Geophys. Res.-Atmos. 123, 12180–12193.
Iqbal, M., 1983. An Introduction to Solar Radiation. Academic Press Canda, Toronto.
Janjai, S., Pankaew, P., Laksanaboonsong, J., 2009. A model for calculating hourly global solar radiation from satellite data in the tropics. Appl. Energy 86, 1450–1457.
Jin, R., Li, X., Liu, S.M., 2017. Understanding the heterogeneity of soil moisture and evapotranspiration using multiscale observations from satellites, airborne sensors, and a ground-based observation matrix. IEEE Geosci. Remote Sens. Lett. 14, 2132–2136.
Kato, S., Loeb, N.G., Rose, F.G., Doelling, D.R., Rutan, D.A., Caldwell, T.E., Yu, L.S., Weller, R.A., 2013. Surface irradiances consistent with CERES-derived top-of-atmosphere shortwave and longwave irradiances. J. Clim. 26, 2719–2740.
Kaufman, Y.J., Wald, A.E., Remer, L.A., Gao, B.C., Li, R.R., Flynn, L., 1997. The MODIS 2.1-mu m channel - correlation with visible reflectance for use in remote sensing of aerosol. IEEE Trans. Geosci. Remote Sens. 35, 1286–1298.
Kim, H.Y., Liang, S.L., 2010. Development of a hybrid method for estimating land surface shortwave net radiation from MODIS data. Remote Sens. Environ. 114, 2393–2402.
King, M.D., Kaufman, Y.J., Tanre, D., Nakajima, T., 1999. Remote sensing of tropospheric aerosols from space: past, present, and future. Bull. Am. Meteorol. Soc. 80, 2229–2259.
Lee, K., Li, Z., Kim, Y.J., Kokhanovsky, A., 2009. Atmosphere aerosol monitoring from satellite observations: a history of three decades. In: Atmospheric and Biological Environmental Monitoring. Springer.
Levy, R.C., Remer, L.A., Mattoo, S., Vermote, E.F., Kaufman, Y.J., 2007. Second-generation operational algorithm: retrieval of aerosol properties over land from inversion of Moderate Resolution Imaging Spectroradiometer spectral reflectance. J. Geophys. Res.-Atmos. 112.
Levy, R.C., Remer, L.A., Kleidman, R.G., Mattoo, S., Ichoku, C., Kahn, R., Eck, T.F., 2010.

Global evaluation of the collection 5 MODIS dark-target aerosol products over land. Atmos. Chem. Phys. 10, 10399–10420.
Li, Z., 1998. Influence of absorbing aerosols on the inference of solar surface radiation budget and cloud absorption. J. Clim. 11, 5–17.
Li, Z., Leighton, H.G., 1991. Scene identification and its effect on cloud radiative forcing in the Arctic. J. Geophys. Res.-Atmos. 96, 9175–9188.
Li, Z., Moreau, L., 1996. A new approach for remote sensing of canopy-absorbed photosynthetically active radiation. 1. Total surface absorption. Remote Sens. Environ. 55, 175–191.
Li, Z., Leighton, H.G., Cess, R.D., 1993a. Surface net solar-radiation estimated from satellite measurements - comparisons with tower observations. J. Clim. 6, 1764–1772.
Li, Z., Leighton, H.G., Masuda, K., Takashima, T., 1993b. Estimation of Sw flux absorbed at the surface from Toa reflected flux. J. Clim. 6, 317–330.
Li, Z., Whitlock, C.H., Charlock, T.P., 1995. Assessment of the global monthly mean surface insolation estimated from satellite measurements using global energy-balance archive data. J. Clim. 8, 315–328.
Li, Z., Moreau, L., Arking, A., 1997a. On solar energy disposition: a perspective from observation and modeling. Bull. Am. Meteorol. Soc. 78, 53–70.
Li, Z., Moreau, L., Cihlar, J., 1997b. Estimation of photosynthetically active radiation absorbed at the surface. J. Geophys. Res.-Atmos. 102, 29717–29727.
Li, Z., Wang, P.C., Cihlar, J., 2000. A simple and efficient method for retrieving surface UV radiation dose rate from satellite. J. Geophys. Res.-Atmos. 105, 5027–5036.
Li, Z., Ackerman, T.P., Wiscombe, W., Stephens, G.L., 2003. Have clouds darkened since 1995? Science 302, 1150–1151.
Li, Z., Wiscombe, W., Stephens, G.L., Ackerman, T.P., 2004. Response to “Disagreement over cloud absorption”. Science 305, 1240.
Li, Z., Cribb, M.C., Chang, F.L., 2005. Natural variability and sampling errors in solar radiation measurements for model validation over the Atmospheric Radiation Measurement Southern Great Plains region. J. Geophys. Res.-Atmos. 110.
Li, X., Pinker, R.T., Wonsick, M.M., Ma, Y.T., 2007. Toward improved satellite estimates of short-wave radiative fluxes focus on cloud detection over snow: 1. Methodology. J. Geophys. Res.-Atmos. 112.
Li, Z., Zhao, X., Kahn, R., Mishchenko, M., Remer, L., Lee, K.H., Wang, M., Laszlo, I., Nakajima, T., Maring, H., 2009. Uncertainties in satellite remote sensing of aerosols and impact on monitoring its long-term trend: a review and perspective. Ann. Geophys. 27, 2755–2770.
Li, X., Cheng, G.D., Liu, S.M., Xiao, Q., Ma, M.G., Jin, R., Che, T., Liu, Q.H., Wang, W.Z., Qi, Y., Wen, J.G., Li, H.Y., Zhu, G.F., Guo, J.W., Ran, Y.H., Wang, S.G., Zhu, Z.L., Zhou, J., Hu, X.L., Xu, Z.W., 2013. Heihe watershed allied telemetry experimental research (HiWATER): scientific objectives and experimental design. Bull. Am. Meteorol. Soc. 94, 1145–1160.
Li, Z., Zhao, F.S., Liu, J.J., Jiang, M.J., Zhao, C.F., Cribb, M., 2014. Opposite effects of absorbing aerosols on the retrievals of cloud optical depth from spaceborne and ground-based measurements. J. Geophys. Res.-Atmos. 119, 5104–5114.
Li, X., Yang, K., Zhou, Y.Z., 2016. Progress in the study of oasis-desert interactions. Agric. For. Meteorol. 230, 1–7.
Liang, S.L., Zheng, T., Liu, R.G., Fang, H.L., Tsay, S.C., Running, S., 2006. Estimation of incident photosynthetically active radiation from Moderate Resolution Imaging Spectrometer data. J. Geophys. Res.-Atmos. 111.
Liang, S., Zhang, X., Xiao, Z., Cheng, J., Liu, Q., Zhao, X., 2014. Global LAnd Surface Satellite (GLASS) Products. Springer.
Liang, S.L., Wang, D.D., He, T., Yu, Y.Y., 2019. Remote sensing of earth's energy budget: synthesis and review. Int. J. Digital Earth 12, 737–780.
Linares-Rodriguez, A., Ruiz-Arias, J.A., Pozo-Vazquez, D., Tovar-Pescador, J., 2013. An artificial neural network ensemble model for estimating global solar radiation from Meteosat satellite images. Energy 61, 636–645.
Liou, K.N., 2002. An Introduction to Atmospheric Radiation, second ed. Academic Press.
Liou, K.N., Gu, Y., Leung, L.R., Lee, W.L., Fovell, R.G., 2013. A WRF simulation of the impact of 3-D radiative transfer on surface hydrology over the Rocky Mountains and Sierra Nevada. Atmos. Chem. Phys. 13, 11709–11721.
Liu, F., Li, X., 2017. Formulation of scale transformation in a stochastic data assimilation framework. Nonlinear Process. Geophys. 24, 279–291.
Liu, S.M., Xu, Z.W., Song, L.S., Zhao, Q.Y., Ge, Y., Xu, T.R., Ma, Y.F., Zhu, Z.L., Jia, Z.Z., Zhang, F., 2016. Upscaling evapotranspiration measurements from multi-site to the satellite pixel scale over heterogeneous land surfaces. Agric. For. Meteorol. 230, 97–113.
Liu, H.L., Tang, S.H., Hu, J.Y., Zhang, S.L., Deng, X.B., 2017. An improved physical split-window algorithm for precipitable water vapor retrieval exploiting the water vapor channel observations. Remote Sens. Environ. 194, 366–378.
Loeb, N.G., Wielicki, B.A., 2016. Satellites and satellite remote sensing: Earth's radiation budget. In: Encyclopedia of Atmospheric Sciences, 2nd edition. .
Lu, N., Liu, R.G., Liu, J.Y., Liang, S.L., 2010. An algorithm for estimating downward shortwave radiation from GMS 5 visible imagery and its evaluation over China. J. Geophys. Res.-Atmos. 115.
Lyapustin, A., Wang, Y., Laszlo, I., Kahn, R., Korkin, S., Remer, L., Levy, R., Reid, J.S., 2011. Multiangle implementation of atmospheric correction (MAIAC): 2. Aerosol algorithm. J. Geophys. Res.-Atmos. 116.
Ma, Y., Pinker, R.T., 2012. Modeling shortwave radiative fluxes from satellites. J. Geophys. Res.-Atmos. 117.
Margulis, S.A., Wood, E.F., Troch, P.A., 2006. The terrestrial water cycle: modeling and data assimilation across catchment scales - introduction. J. Hydrometeorol. 7, 309–311.
Mayer, B., Kylling, A., 2005. Technical note: the libRadtran software package for radiative transfer calculations - description and examples of use. Atmos. Chem. Phys. 5, 1855–1877.
Mayer, B., Kylling, A., Emde, C., Buras, R., Hamann, U., Gasteiger, J., Richter, B., 2016. libRadtran User's Guide.
Mefti, A., Adane, A., Bouroubi, M.Y., 2008. Satellite approach based on cloud cover classification: estimation of hourly global solar radiation from meteosat images. Energy Convers. Manag. 49, 652–659.
Moreau, L., Li, Z.Q., 1996. A new approach for remote sensing of canopy absorbed photosynthetically active radiation. 2. Proportion of canopy absorption. Remote Sens. Environ. 55, 192–204.
Mueller, R.W., Dagestad, K.F., Ineichen, P., Schroedter-Homscheidt, M., Cros, S., Dumortier, D., Kuhlemann, R., Olseth, J.A., Piernavieja, G., Reise, C., Wald, L., Heinemann, D., 2004. Rethinking satellite-based solar irradiance modelling - the SOLIS clear-sky module. Remote Sens. Environ. 91, 160–174.
Mueller, R.W., Matsoukas, C., Gratzki, A., Behr, H.D., Hollmann, R., 2009. The CM-SAF operational scheme for the satellite based retrieval of solar surface irradiance - a LUT based eigenvector hybrid approach. Remote Sens. Environ. 113, 1012–1024.
Muller, R., Pfeifroth, U., Traeger-Chatterjee, C., Trentmann, J., Cremer, R., 2015. Digging the METEOSAT treasure-3 decades of solar surface radiation. Remote Sens. 7, 8067–8101.
Oinas, V., Lacis, A.A., Rind, D., Shindell, D.T., Hansen, J.E., 2001. Radiative cooling by stratospheric water vapor: big differences in GCM results. Geophys. Res. Lett. 28, 2791–2794.
Perez, R., Ineichen, P., Moore, K., Kmiecik, M., Chain, C., George, R., Vignola, F., 2002. A new operational model for satellite-derived irradiances: description and validation. Sol. Energy 73, 307–317.
Perez, R., Cebecauer, T., Suri, M., 2013. Semi-empirical satellite models. In: Kleissl, J. (Ed.), Solar Energy Forecasting and Resource Assessment. Academic press, pp. 21–48.
Perez, R., Schlemmer, J., Hemker, K., Kivalov, S., Kankiewicz, A., Gueymard, C., 2015. Satellite-to-irradiance modeling - a new version of the SUNY model. In: IEEE 42nd Photovoltaic Specialist Conference.
Perez, R., Schlemmer, J., Kankiewicz, A., Dise, J., Tadese, A., Hoff, T., 2017. Detecting calibration drift at ground truth stations: a demonstration of satellite irradiance models' accuracy. In: IEEE 44th Photovoltaic Specialist Conference.
Pinker, R.T., Laszlo, I., 1992. Modeling surface solar irradiance for satellite applications on a global scale. J. Appl. Meteorol. 31, 194–211.
Pinker, R.T., Frouin, R., Li, Z., 1995. A review of satellite methods to derive surface shortwave irradiance. Remote Sens. Environ. 51, 108–124.
Pinker, R.T., Tarpley, J.D., Laszlo, I., Mitchell, K.E., Houser, P.R., Wood, E.F., Schaake, J.C., Robock, A., Lohmann, D., Cosgrove, B.A., Sheffield, J., Duan, Q.Y., Luo, L.F., Higgins, R.W., 2003. Surface radiation budgets in support of the GEWEX Continental-Scale International Project (GCIP) and the GEWEX Americas Prediction Project (GAPP), including the North American Land Data Assimilation System (NLDAS) Project. J. Geophys. Res.-Atmos. 108.
Pinker, R.T., Zhang, B., Dutton, E.G., 2005. Do satellites detect trends in surface solar radiation? Science 308, 850–854.
Pinker, R.T., Li, X., Meng, W., Yegorova, E.A., 2007. Toward improved satellite estimates of short-wave radiative fluxes - focus on cloud detection over snow: 2. Results. J. Geophys. Res.-Atmos. 112.
Pinker, R.T., Wang, H.M., Grodsky, S.A., 2009. How good are ocean buoy observations of radiative fluxes? Geophys. Res. Lett. 36.
Platnick, S., Li, J.Y., King, M.D., Gerber, H., Hobbs, P.V., 2001. A solar reflectance method for retrieving the optical thickness and droplet size of liquid water clouds over snow and ice surfaces. J. Geophys. Res.-Atmos. 106, 15185–15199.
Platnick, S., King, M.D., Ackerman, S.A., Menzel, W.P., Baum, B.A., Riedi, J.C., Frey, R.A., 2003. The MODIS cloud products: algorithms and examples from Terra. IEEE Trans. Geosci. Remote Sens. 41, 459–473.
Platnick, S., King, M.D., Meyer, K.G., Wind, G., Amarasinghe, N., Marchant, B., Arnold, G.T., Zhang, Z.B., Hubanks, P.A., 2015. MODIS Cloud Optical Properties: User Guide for the Collection 6 Level-2 MOD06/MYD06 Product and Associated Level-3 Datasets. Earth Sciences Division, NASA Goddard Space Flight Center, Greenbelt, MD.
Platnick, S., Meyer, K.G., King, M.D., Wind, G., Amarasinghe, N., Marchant, B., Arnold, G.T., Zhang, Z.B., Hubanks, P.A., Holz, R.E., Yang, P., Ridgway, W.L., Riedi, J., 2017. The MODIS cloud optical and microphysical products: collection 6 updates and examples from terra and aqua. IEEE Trans. Geosci. Remote Sens. 55, 502–525.
Qin, J., Chen, Z.Q., Yang, K., Liang, S.L., Tang, W.J., 2011. Estimation of monthly-mean daily global solar radiation based on MODIS and TRMM products. Appl. Energy 88, 2480–2489.
Qin, J., Tang, W.J., Yang, K., Lu, N., Niu, X.L., Liang, S.L., 2015. An efficient physically based parameterization to derive surface solar irradiance based on satellite atmospheric products. J. Geophys. Res.-Atmos. 120, 4975–4988.
Qu, Z., Oumbe, A., Blanc, P., Lefevre, M., Wald, L., 2012. A new method for assessing surface solar irradiance: Heliosat-4. In: Geophysical Research Abstracts.
Raisanen, P., 2002. Two-stream approximations revisited: a new improvement and tests with GCM data. Q. J. R. Meteorol. Soc. 128, 2397–2416.
Ramanathan, V., Subasilar, B., Zhang, G.J., Conant, W., Cess, R.D., Kiehl, J.T., Grassl, H., Shi, L., 1995. Warm pool heat-budget and shortwave cloud forcing - a missing physics. Science 267, 499–503.
Rasool, S.I., 1964. Global distribution of net energy balance of atmosphere from Tiros radiation data. Science 143, 567.
Ricciardelli, E., Romano, F., Cuomo, V., 2008. Physical and statistical approaches for cloud identification using Meteosat second generation-spinning enhanced visible and infrared imager data. Remote Sens. Environ. 112, 2741–2760.
Rigollier, C., Lefevre, M., Wald, L., 2004. The method Heliosat-2 for deriving shortwave solar radiation from satellite images. Sol. Energy 77, 159–169.
Riihela, A., Key, J.R., Meirink, J.F., Munneke, P.K., Palo, T., Karlsson, K.G., 2017. An intercomparison and validation of satellite-based surface radiative energy flux estimates over the Arctic. J. Geophys. Res.-Atmos. 122, 4829–4848.
Rossow, W.B., Schiffer, R.A., 1999. Advances in understanding clouds from ISCCP. Bull.

Am. Meteorol. Soc. 80, 2261–2287.
Rossow, W.B., Zhang, Y.C., 1995. Calculation of surface and top of atmosphere radiative fluxes from physical quantities based on Isccp data sets. 2. Validation and first results. J. Geophys. Res.-Atmos. 100, 1167–1197.
Schiffer, R.A., Rossow, W.B., 1983. The international-satellite-cloud-climatology-project (Isccp) - the 1st project of the world-climate-research-programme. Bull. Am. Meteorol. Soc. 64, 779–784.
Schiffer, R., Rossow, W., 1985. ISCCP global radiance data set: a new resource for climate research. Bull. Am. Meteorol. Soc. 66, 1498–1505.
Schmetz, J., 1989. Towards a surface radiation climatology: retrieval of downward irradiances from satellites. Atmos. Res. 23, 287–321.
Schwarz, M., Folini, D., Hakuba, M.Z., Wild, M., 2018. From point to area: worldwide assessment of the representativeness of monthly surface solar radiation records. J. Geophys. Res.-Atmos. 123, 13857–13874.
Shi, Q.Q., Liang, S.L., 2013a. Characterizing the surface radiation budget over the Tibetan Plateau with ground-measured, reanalysis, and remote sensing data sets: 1. Methodology. J. Geophys. Res.-Atmos. 118, 9642–9657.
Shi, Q.Q., Liang, S.L., 2013b. Characterizing the surface radiation budget over the Tibetan Plateau with ground-measured, reanalysis, and remote sensing data sets: 2. Spatiotemporal analysis. J. Geophys. Res.-Atmos. 118, 8921–8934.
Slingo, A., 1989. A GCM parameterization for the shortwave radiative properties of water clouds. J. Atmos. Sci. 46, 1419–1427.
Stengel, M.S., Kniffka, A.K., Meirink, J.F.M., Lockhoff, M.L., Tan, J.T., Hollmann, R.H., 2014. CLAAS: the CM SAF cloud property data set using SEVIRI. Atmos. Chem. Phys. 14, 4297–4311.
Stephens, G.L., Ackerman, S., Smith, E.A., 1984. A shortwave parameterization revised to improve cloud absorption. J. Atmos. Sci. 41, 687–690.
Stephens, G.L., Li, J.L., Wild, M., Clayson, C.A., Loeb, N., Kato, S., L'Ecuyer, T., Stackhouse, P.W., Lebsock, M., Andrews, T., 2012. An update on Earth's energy balance in light of the latest global observations. Nat. Geosci. 5, 691–696.
Suttles, J.T., Ohring, G., 1986. Report of the workshop on surface radiation budget for climate applications. WCRP WC-119. In: World Meteorological Organization Tech. Doc. WMO/TD, pp. 109.
Tang, W.J., Qin, J., Yang, K., Liu, S.M., Lu, N., Niu, X.L., 2016. Retrieving high-resolution surface solar radiation with cloud parameters derived by combining MODIS and MTSAT data. Atmos. Chem. Phys. 16, 2543–2557.
Tarpley, J.D., 1979. Estimating incident solar-radiation at the surface from geostationary satellite data. J. Appl. Meteorol. 18, 1172–1181.
Trentmann, J., Kothe, S., 2016. Algorithm theoretical baseline document (ATBD) CLARA-A2 surface radiation products. In: EUMETSAT Satellite Application Facility on Climate Monitoring.
Van Laake, P.E., Sanchez-Azofeifa, G.A., 2004. Simplified atmospheric radiative transfer modelling for estimating incident PAR using MODIS atmosphere products. Remote Sens. Environ. 91, 98–113.
Vindel, J.M., Navarro, A.A., Valenzuela, R.X., Ramirez, L., 2016. Temporal scaling analysis of irradiance estimated from daily satellite data and numerical modelling. Atmos. Res. 181, 154–162.
Vonderhaar, T.H., Suomi, V.E., 1969. Satellite observations of earths radiation budget. Science 163, 667–669.
Voyant, C., Notton, G., Kalogirou, S., Nivet, M.L., Paoli, C., Motte, F., Fouilloy, A., 2017. Machine learning methods for solar radiation forecasting: a review. Renew. Energy 105, 569–582.
Wang, H., Pinker, R.T., 2009. Shortwave radiative fluxes from MODIS: model development and implementation. J. Geophys. Res.-Atmos. 114.
Wang, P.C., Li, Z.Q., Cihlar, J., Wardle, D.I., Kerr, J., 2000. Validation of an UV inversion algorithm using satellite and surface measurements. J. Geophys. Res.-Atmos. 105, 5037–5048.
Wang, K.C., Ma, Q., Wang, X.Y., Wild, M., 2014. Urban impacts on mean and trend of surface incident solar radiation. Geophys. Res. Lett. 41, 4664–4668.
Wang, S.G., Li, X., Ge, Y., Jin, R., Ma, M.G., Liu, Q.H., Wen, J.G., Liu, S.M., 2016. Validation of regional-scale remote sensing products in China: from site to network. Remote Sens. 8.
Whitlock, C.H., Charlock, T., Staylor, W., Pinker, R., Laszlo, I., Ohmura, A., Gilgen, H., Konzelman, T., DiPasquale, R., Moats, C., 1995. First global WCRP shortwave surface radiation budget dataset. Bull. Am. Meteorol. Soc. 76, 905–922.
Wild, M., Folini, D., Schar, C., Loeb, N., Dutton, E.G., Konig-Langlo, G., 2013. The global energy balance from a surface perspective. Clim. Dyn. 40, 3107–3134.
Wild, M., Ohmura, A., Schar, C., Muller, G., Hakuba, M.Z., Mystakidis, S., Arsenovic, P., Sanchez-Lorenzo, A., 2017. The Global Energy Balance Archive (GEBA): a database for the worldwide measured surface energy fluxes. Radiation Processes in the Atmosphere and Ocean 1810.
Wood, N., 2008. Level 2B Radar-visible Optical Depth Cloud Water Content (2B-CWC-RVOD) Process Description Document. Department of Atmospheric Science, Colorado State University.
Wu, F.T., Fu, C.B., 2011. Assessment of GEWEX/SRB version 3.0 monthly global radiation dataset over China. Meteorog. Atmos. Phys. 112, 155–166.
Wyser, K., O'Hirok, W., Gautier, C., Jones, C., 2002. Remote sensing of surface solar irradiance with corrections for 3-D cloud effects. Remote Sens. Environ. 80, 272–284.
Wyser, K., O'Hirok, W., Gautier, C., 2005. A simple method for removing 3-D radiative effects in satellite retrievals of surface irradiance. Remote Sens. Environ. 94, 335–342.
Xia, X.A., Wang, P.C., Chen, H.B., Liang, F., 2006. Analysis of downwelling surface solar radiation in China from National Centers for Environmental Prediction reanalysis, satellite estimates, and surface observations. J. Geophys. Res.-Atmos. 111.
Xin, J.Y., Wang, L.L., Wang, Y.S., Li, Z.Q., Wang, P.C., 2011. Trends in aerosol optical properties over the Bohai Rim in Northeast China from 2004 to 2010. Atmos. Environ. 45, 6317–6325.
Xu, T.R., Liu, S.M., Xu, L., Chen, Y.J., Jia, Z.Z., Xu, Z.W., Nielson, J., 2015. Temporal upscaling and reconstruction of thermal remotely sensed instantaneous evapotranspiration. Remote Sens. 7, 3400–3425.
Yang, K., Huang, G.W., Tamai, N., 2001. A hybrid model for estimating global solar radiation. Sol. Energy 70, 13–22.
Yang, K., Koike, T., Stackhouse, P., Mikovitz, C., Cox, S.J., 2006a. An assessment of satellite surface radiation products for highlands with Tibet instrumental data. Geophys. Res. Lett. 33.
Yang, K., Koike, T., Ye, B.S., 2006b. Improving estimation of hourly, daily, and monthly solar radiation by importing global data sets. Agric. For. Meteorol. 137, 43–55.
Yang, K., Pinker, R.T., Ma, Y., Koike, T., Wonsick, M.M., Cox, S.J., Zhang, Y., Stackhouse, P., 2008. Evaluation of satellite estimates of downward shortwave radiation over the Tibetan Plateau. J. Geophys. Res.-Atmos. 113.
Yang, P., Bi, L., Baum, B.A., Liou, K.N., Kattawar, G.W., Mishchenko, M.I., Cole, B., 2013. Spectrally consistent scattering, absorption, and polarization properties of atmospheric ice crystals at wavelengths from 0.2 to 100 mu m. J. Atmos. Sci. 70, 330–347.
Zhang, Y.C., Rossow, W.B., Lacis, A.A., 1995. Calculation of surface and top of atmosphere radiative fluxes from physical quantities based on Isccp data sets. 1. Method and sensitivity to input data uncertainties. J. Geophys. Res.-Atmos. 100, 1149–1165.
Zhang, Y., Li, Z.Q., Macke, A., 2002. Retrieval of surface solar radiation budget under ice cloud sky: uncertainty analysis and parameterization. J. Atmos. Sci. 59, 2951–2965.
Zhang, Y.C., Rossow, W.B., Lacis, A.A., Oinas, V., Mishchenko, M.I., 2004. Calculation of radiative fluxes from the surface to top of atmosphere based on ISCCP and other global data sets: refinements of the radiative transfer model and the input data. J. Geophys. Res.-Atmos. 109.
Zhang, T.P., Stackhouse, P.W., Gupta, S.K., Cox, S.J., Mikovitz, J.C., Hinkelman, L.M., 2013. The validation of the GEWEX SRB surface shortwave flux data products using BSRN measurements: a systematic quality control, production and application approach. J. Quant. Spectrosc. Radiat. Transf. 122, 127–140.
Zhang, X.T., Liang, S.L., Zhou, G.Q., Wu, H.R., Zhao, X., 2014. Generating Global LAnd Surface Satellite incident shortwave radiation and photosynthetically active radiation products from multiple satellite data. Remote Sens. Environ. 152, 318–332.
Zhang, X.T., Liang, S.L., Wild, M., Jiang, B., 2015. Analysis of surface incident shortwave radiation from four satellite products. Remote Sens. Environ. 165, 186–202.
Zhang, X.T., Liang, S.L., Wang, G.X., Yao, Y.J., Jiang, B., Cheng, J., 2016. Evaluation of the reanalysis surface incident shortwave radiation products from NCEP, ECMWF, GSFC, and JMA using satellite and surface observations. Remote Sens. 8.
Zhang, J.Y., Zhao, L., Deng, S., Xu, W.C., Zhang, Y., 2017. A critical review of the models used to estimate solar radiation. Renew. Sust. Energ. Rev. 70, 314–329.
Zhang, Y., He, T., Liang, S.L., Wang, D.D., 2018. Estimation of all-sky instantaneous surface incident shortwave radiation from Moderate Resolution Imaging Spectroradiometer data using optimization method. Remote Sens. Environ. 209, 468–479.
Zhao, L., Lee, X.H., Liu, S.D., 2013. Correcting surface solar radiation of two data assimilation systems against FLUXNET observations in North America. J. Geophys. Res.-Atmos. 118, 9552–9564.